Soft Drop

Andrew J. Larkoski,[a] **Simone Marzani,**[b] **Gregory Soyez,**[c] **and Jesse Thaler**[a]

[a]*Center for Theoretical Physics, Massachusetts Institute of Technology, Cambridge, MA 02139, USA*
[b]*Institute for Particle Physics Phenomenology, Durham University, South Road, Durham DH1 3LE, United Kingdom*
[c]*IPhT, CEA Saclay, CNRS URA 2306, F-91191 Gif-sur-Yvette, France*
E-mail: larkoski@mit.edu, simone.marzani@durham.ac.uk, gregory.soyez@cea.fr, jthaler@mit.edu

ABSTRACT: We introduce a new jet substructure technique called "soft drop declustering", which recursively removes soft wide-angle radiation from a jet. The soft drop algorithm depends on two parameters—a soft threshold z_{cut} and an angular exponent β—with the $\beta = 0$ limit corresponding roughly to the (modified) mass drop procedure. To gain an analytic understanding of soft drop and highlight the β dependence, we perform resummed calculations for three observables on soft-dropped jets: the energy correlation functions, the groomed jet radius, and the energy loss due to soft drop. The $\beta = 0$ limit of the energy loss is particularly interesting, since it is not only "Sudakov safe" but also largely insensitive to the value of the strong coupling constant. While our calculations are strictly accurate only to modified leading-logarithmic order, we also include a discussion of higher-order effects such as multiple emissions and (the absence of) non-global logarithms. We compare our analytic results to parton shower simulations and find good agreement, and we also estimate the impact of non-perturbative effects such as hadronization and the underlying event. Finally, we demonstrate how soft drop can be used for tagging boosted W bosons, and we speculate on the potential advantages of using soft drop for pileup mitigation.

arXiv:1402.2657v2 [hep-ph] 13 May 2014

Contents

1 Introduction

The study of jet substructure has significantly matured over the past five years [1–3], with numerous techniques proposed to tag boosted objects [4–46], distinguish quark from gluon jets [44, 47–51], and mitigate the effects of jet contamination [6, 52–61]. Many of these techniques have found successful applications in jet studies at the Large Hadron Collider (LHC) [50, 62–89], and jet substructure is likely to become even more relevant with the anticipated increase in energy and luminosity for Run II of the LHC.

In addition to these phenomenological and experimental studies of jet substructure, there is a growing catalog of first-principles calculations using perturbative QCD (pQCD). These include more traditional jet mass and jet shape distributions [90–95] as well as more sophisticated substructure techniques [44, 59, 60, 96–103]. Recently, Refs. [59, 60] considered the analytic behavior of three of the most commonly used jet tagging/grooming methods—trimming [53], pruning [54, 55], and mass drop tagging [6]. Focusing on groomed jet mass distributions, this study showed how their qualitative and quantitative features could be understood with the help of logarithmic resummation. Armed with this analytic understanding of jet substructure, the authors of Ref. [59] developed the modified mass drop tagger (mMDT) which exhibits some surprising features in the resulting groomed jet mass distribution, including the absence of Sudakov double logarithms, the absence of non-global logarithms [104], and a high degree of insensitivity to non-perturbative effects.

In this paper, we introduce a new tagging/grooming method called "soft drop declustering", with the aim of generalizing (and in some sense simplifying) the mMDT procedure. Like any grooming method, soft drop declustering removes wide-angle soft radiation from a jet in order to mitigate the effects of contamination from initial state radiation (ISR), underlying event (UE), and multiple hadron scattering (pileup). Given a jet of radius R_0 with only two constituents, the soft drop procedure removes the softer constituent unless

$$\text{Soft Drop Condition:} \quad \frac{\min(p_{T1}, p_{T2})}{p_{T1} + p_{T2}} > z_{\text{cut}} \left(\frac{\Delta R_{12}}{R_0} \right)^{\beta}, \tag{1.1}$$

where p_{Ti} are the transverse momenta of the constituents with respect to the beam, ΔR_{12} is their distance in the rapidity-azimuth plane, z_{cut} is the soft drop threshold, and β is an angular exponent. By construction, Eq. (1.1) fails for wide-angle soft radiation. The degree of jet grooming is controlled by z_{cut} and β, with $\beta \to \infty$ returning back an ungroomed jet. As we explain in Sec. 2, this procedure can be extended to jets with more than two constituents with the help of recursive pairwise declustering.[1]

Following the spirit of Ref. [59], the goal of this paper is to understand the analytic behavior of the soft drop procedure, particularly as the angular exponent β is varied. There are two different regimes of interest. For $\beta > 0$, soft drop declustering removes soft radiation

---

[1]The soft drop procedure takes some inspiration from the "semi-classical jet algorithm" [58], where a variant of Eq. (1.1) with $z_{\text{cut}} = 1/2$ and $\beta = 3/2$ is tested at each stage of recursive clustering (unlike declustering considered here).

from a jet while still maintaining a fraction (controlled by β) of the soft-collinear radiation. One of the consequences is that the soft drop procedure gives infrared/collinear (IRC) safe results even on a jet with just one constituent. In this regime, soft drop acts like a "groomer", meaning that it changes the constituents of a jet without affecting the overall jet production cross section. For $\beta < 0$, soft drop declustering can remove both soft and collinear radiation. For a jet to pass the soft drop procedure, it must have at least two constituents satisfying Eq. (1.1). Thus, in this regime, soft drop acts like a "tagger", since it vetoes jets that do not have two well-separated hard prongs. Roughly speaking, the boundary $\beta = 0$ corresponds to mMDT, which acts like a tagger at any fixed-order in an α_s expansion, but can be thought of as a "Sudakov safe" [105] groomer when all orders in α_s are considered.

To demonstrate the behavior of the soft drop procedure, we will present three calculations performed on soft-dropped jets.

- *Energy correlation functions.* The generalized energy correlation functions (ECF) were introduced in Ref. [44], where $\mathrm{ECF}\,(N, \alpha)$ corresponds to an N-point correlation function with angular exponent α. In this paper, we will focus on the 2-point correlator through the combination $C_1^{(\alpha)} \equiv \mathrm{ECF}\,(2, \alpha)\,/\mathrm{ECF}\,(1, \alpha)^2$ (see also Refs. [32, 106]). For a jet with two constituents,

$$C_1^{(\alpha)} \simeq \frac{p_{T1}\,p_{T2}}{(p_{T1} + p_{T2})^2} \left(\frac{\Delta R_{12}}{R_0} \right)^\alpha, \tag{1.2}$$

  where we have added an extra R_0 normalization factor for later convenience. The value $\alpha = 2$ is related to jet thrust/mass [7, 91, 107], $\alpha = 1$ is related to jet broadening/girth/width [25, 47], and arbitrary $\alpha > 0$ is related to the recoil-free angularities [102]. In Sec. 3, we calculate $C_1^{(\alpha)}$ in the modified leading logarithmic (MLL) approximation, which accounts for all terms $\alpha_s^n L^{2n-q}$ with $q = 0, 1$ and $L \equiv \log(1/C_1^{(\alpha)})$ in the expansion of the $C_1^{(\alpha)}$ cumulative distribution. We will also compute higher-order effects due to multiple emissions and we will find an interesting interplay between the ECF exponent α and the soft drop exponent β, especially as relates to non-global logarithms.

- *Groomed jet radius.* The soft drop declustering procedure terminates when Eq. (1.1) is satisfied, and the corresponding ΔR_{12} gives the effective radius R_g of the groomed jet. Roughly speaking, the active jet area [108] is $\simeq \pi R_g^2$. In Sec. 4, we calculate the R_g distribution to MLL accuracy to gain an understanding of how the soft drop procedure might perform in a pileup environment.

- *Jet energy drop.* Strictly speaking, the groomed jet energy distribution after mMDT (i.e. $\beta = 0$) is not IRC safe. One of the motivations for introducing the generalized soft drop procedure with $\beta > 0$ is to have a method (in the same spirit of trimming [53]) that gives IRC safe distributions for any (otherwise) IRC safe observable measured on groomed jets. In Sec. 5, we calculate the fractional drop in the jet energy after the soft drop procedure to MLL accuracy, including higher-order corrections due to multiple

emissions. Intriguingly, we will find that the $\beta \to 0$ limit is "Sudakov safe" [105], and the resulting jet energy drop spectrum is *independent* of α_s in the fixed coupling approximation.

While the focus of this paper is on the analytic properties of the soft drop procedure, we will cross check our results using parton shower Monte Carlo simulations. In addition to these analytic studies, we will perform a Monte Carlo study of non-perturbative corrections (hadronization and UE) in Sec. 6, and estimate the tagging performance of soft drop for boosted W bosons in Sec. 7. We present our conclusions in Sec. 8.

2 Soft Drop Declustering

2.1 Definition

The starting point for soft drop declustering is a jet with characteristic radius R_0. For definiteness, we will always consider jets defined with the anti-k_t algorithm [109], but other jet algorithms would work equally well. We then recluster the jet constituents using the Cambridge-Aachen (C/A) algorithm [110, 111] to form a pairwise clustering tree with an angular-ordered structure.

The soft drop declustering procedure depends on two parameters, a soft threshold z_{cut} and an angular exponent β, and is implemented as follows:

1. Break the jet j into two subjets by undoing the last stage of C/A clustering. Label the resulting two subjets as j_1 and j_2.

2. If the subjets pass the soft drop condition $\left(\frac{\min(p_{T1}, p_{T2})}{p_{T1} + p_{T2}} > z_{\text{cut}} \left(\frac{\Delta R_{12}}{R_0} \right)^\beta \text{, see Eq. } (1.1) \right)$ then deem j to be the final soft-drop jet. (Optionally, one could also impose the mass-drop condition $\max(m_1, m_2) < \mu \, m$ as in Ref. [6], but we will not use that here.)

3. Otherwise, redefine j to be equal to subjet with larger p_T and iterate the procedure.

4. If j is a singleton and can no longer be declustered, then one can either remove j from consideration ("tagging mode") or leave j as the final soft-drop jet ("grooming mode").

By building a C/A tree, we can apply the pairwise soft drop condition from Eq. (1.1) to a jet with more than two constituents. Tagging mode is only IRC safe for $\beta \leq 0$ whereas grooming mode is only IRC safe for $\beta > 0$. In this paper, we will typically consider $z_{\text{cut}} \simeq 0.1$ but we will explore a wide range of β values.[2]

The above algorithm can be thought of as a generalization of the (modified) mass-drop tagger (mMDT) [6, 59], with $\beta = 0$ roughly corresponding to mMDT itself. There are,

---

[2]Throughout this paper, we will assume that $\Delta R_{12} < R_0$ at every stage of the declustering, such that the algorithm returns the whole jet in the $\beta \to \infty$ limit. In practice, it is possible for a jet of characteristic radius R_0 to have $\Delta R_{12} > R_0$ when reclustered with C/A, and in that case we simply apply step 2 without change, such that wide angle emissions can still be vetoed even in the $\beta \to \infty$ limit.

however, a few important differences. First, soft drop declustering does not require a mass drop condition (or equivalently, the mass drop parameter μ is set to unity). As shown in Ref. [59], the mass drop condition is largely irrelevant for understanding the analytic behavior of mMDT on quark/gluon jets, so we have decided not to include it in the definition here. Second, we note that the $\beta = 0$ limit corresponds to a mMDT variant where step 2 is implemented directly on the transverse momentum fractions of subjets, rather than indirectly through a ratio of a k_t-distance to a mass [59]. Of course, the two give the same behavior in the small $\min(p_{T1}, p_{T2})/(p_{T1} + p_{T2})$ limit, but Eq. (1.1) makes it obvious that the soft drop condition drops soft radiation (true to its name). Finally and most importantly, for $\beta \neq 0$, the soft drop condition involves a relation between energies and angular distances, rather than just energies as is the case for $\beta = 0$. It is this additional angular dependence (exploited by the exponent β) that we wish to highlight in this paper.

As mentioned in footnote 1, the soft drop condition takes some inspiration from the "semi-classical jet algorithm" [58]. The semi-classical algorithm is a pairwise clustering algorithm that only allows mergings which satisfy

$$\text{Semi-classical Condition:} \quad \frac{\min(m_{T1}, m_{T2})}{m_{T1} + m_{T2}} > \frac{1}{2} \left(\frac{\Delta R_{12}}{R_0} \right)^{3/2}, \tag{2.1}$$

where $m_{Ti} = \sqrt{m_i^2 + p_{Ti}^2}$. Apart from the change of $p_{Ti} \to m_{Ti}$, the semi-classical condition looks like the soft drop condition with $\beta = 3/2$ and $z_{\text{cut}} = 1/2$, but there is an important difference. For semi-classical jets, one is recursively clustering a jet using a novel measure. For soft-drop jets, one is taking an existing jet defined with a traditional algorithm and using soft drop declustering to groom away soft wide-angle emissions. Of course, the distinction between clustering and declustering is irrelevant for a jet with only two constituents, but it is very important for our analytic calculations which only apply to declustering of a C/A tree.[3]

2.2 Dependence on β

Before studying the analytic behavior of soft-drop distributions in detail, it is worth making a few general comments about the expected β dependence. For simplicity of discussion, we will work with central jets (i.e. rapidity $y = 0$) with small radius ($R_0 \ll 1$). This way, we can freely exchange transverse momentum p_T for energy E, as well as rapidity-azimuth distance R for opening angle θ. All of the results of this paper extend to non-zero rapidity as well, up to power corrections in the jet radius, which we neglect.

In Fig. 1, we show the phase space for a single gluon emission from an eikonal hard quark/gluon on the $(\log \frac{1}{z}, \log \frac{R_0}{\theta})$ plane, where $0 \leq z \leq 1$ is the energy fraction and $0 \leq \theta \leq R_0$ is the angle of the emission. We have labeled three modes in the phase space: soft, soft-collinear, and collinear. For this paper, we define the various modes in terms of their z

---

[3]In principle, it is possible to use any of the generalized k_t algorithms [112, 113] to perform the soft drop declustering. The choice of C/A is motivated by the approximate angular ordering of emissions in the parton shower.
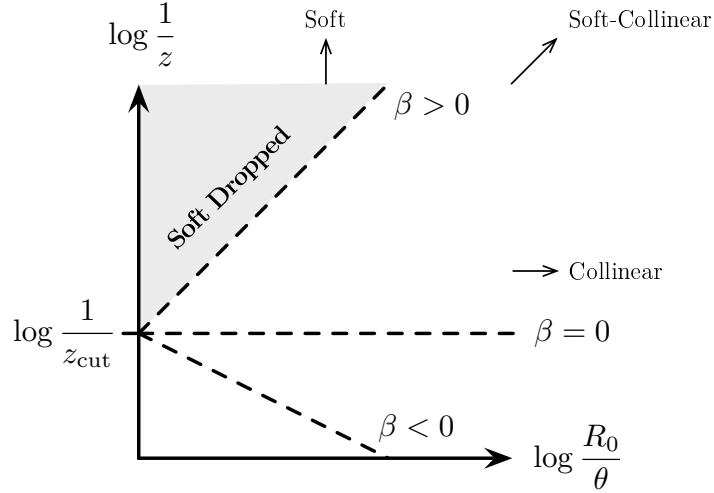
Figure 1: Phase space for emissions on the $(\log\frac{1}{z}, \log\frac{R_0}{\theta})$ plane. In the strongly-ordered limit, emissions above the dashed line (Eq. (2.2)) are vetoed by the soft drop condition. For $\beta > 0$, soft emissions are vetoed while much of the soft-collinear region is maintained. For $\beta = 0$ (mMDT), both soft and soft-collinear emissions are vetoed. For $\beta < 0$, all (two-prong) singularities are regulated by the soft drop procedure.

and θ behavior:

$$\begin{aligned}
\text{soft modes:} & \quad z \to 0, \ \theta = \text{constant}, \\
\text{soft-collinear modes:} & \quad z \to 0, \ \theta \to 0, \\
\text{collinear modes:} & \quad z = \text{constant}, \ \theta \to 0.
\end{aligned}$$

No relative scaling is assumed between energy fraction z and splitting angle θ for soft-collinear modes. In these logarithmic coordinates, the emission probability is flat in the soft-collinear limit. In the soft limit, the soft drop criteria reduces to

$$z > z_{\text{cut}} \left(\frac{\theta}{R_0}\right)^\beta \quad \Rightarrow \quad \log\frac{1}{z} < \log\frac{1}{z_{\text{cut}}} + \beta \log\frac{R_0}{\theta}. \tag{2.2}$$

Thus, vetoed emissions lie above a straight line of slope β on the $(\log\frac{1}{z}, \log\frac{R_0}{\theta})$ plane, as shown in Fig. 1.

For $\beta > 0$, collinear radiation always satisfies the soft drop condition, so a soft-drop jet still contains all of its collinear radiation. The amount of soft-collinear radiation that satisfies the soft drop condition depends on the relative scaling of the energy fraction z to the angle θ. As $\beta \to 0$, more of the soft-collinear radiation of the jet is removed, and in the $\beta = 0$ (mMDT) limit, all soft-collinear radiation is removed. Therefore, we expect that the coefficient of the double logarithms of observables like groomed jet mass (and $C_1^{(\alpha)}$) will be proportional to β,

when β is small. Similarly, because the soft drop procedure does not change the structure of collinear emissions, observables like the groomed jet energy are IRC safe. Note that running $\beta > 0$ soft drop in tagging mode is not IRC safe, since a jet would (would not) be tagged if it contained two (one) collinear particles.

In the strict $\beta = 0$ or mMDT limit, collinear radiation is only maintained if $z > z_{\text{cut}}$. Because soft-collinear radiation is vetoed, the resulting jet mass (and $C_1^{(\alpha)}$) distributions will only exhibit single logarithms, as emphasized in Refs. [59, 60]. Because the structure of collinear emissions is modified, observables like groomed jet energy are only IRC safe if soft drop is used in tagging mode, since that forces the jet to have a hard two-prong structure, which regulates the collinear singularity. We will see in Sec. 5, however, that $\beta = 0$ grooming mode is still "Sudakov safe" [105].

Finally, for $\beta < 0$, there are no logarithmic structures for observables like groomed jet mass at arbitrarily low values of the observable. Effectively, soft drop with negative β acts like a cut which enforces $C_1^{(\alpha)} > z_{\text{cut}}^{\alpha/|\beta|}$, and this cut regulates the soft-collinear singularities. For example, $\beta = -1$ roughly corresponds to a cut on the relative transverse momentum of the two prongs under scrutiny. Like for $\beta = 0$, $\beta < 0$ is only IRC safe in tagging mode.

3 Energy Correlation Functions after Soft Drop

Generalized energy correlation functions $\text{ECF}\,(N, \alpha)$ and their double ratios $C_{N-1}^{(\alpha)}$ were introduced in Ref. [44] (see also Refs. [32, 106] for $N = 2$). In this paper, we only consider the double ratio for $N = 2$ (hereafter referred to as simply the energy correlation functions):

$$C_1^{(\alpha)} = \frac{\text{ECF}\,(2, \alpha)\,\text{ECF}\,(0, \alpha)}{\text{ECF}\,(1, \alpha)^2}, \tag{3.1}$$

where

$$
\begin{aligned}
\text{ECF}\,(0, \alpha) &= 1, \\
\text{ECF}\,(1, \alpha) &= \sum_{i \in \text{jet}} p_{Ti}, \\
\text{ECF}\,(2, \alpha) &= \sum_{i < j \,\in \text{jet}} p_{Ti}\, p_{Tj} \left(\frac{\Delta R_{ij}}{R_0} \right)^{\alpha}.
\end{aligned}
\tag{3.2}
$$

In this study, we will measure $C_1^{(\alpha)}$ on jets which have been groomed according to the soft-drop declustering described above. We will work to lowest non-trivial order in z_{cut}, such that we can ignore the effect of grooming on $\text{ECF}\,(1, \alpha)$. As stated above, we will focus on central jets $(y = 0)$ and assume $R_0 \ll 1$. In those limits,

$$C_1^{(\alpha)} \simeq \sum_{i < j} z_i z_j \left(\frac{\theta_{ij}}{R_0} \right)^{\alpha}, \tag{3.3}$$

where $z_i \simeq E_i / E_{\text{jet}}$ is the energy fraction carried by particle i, and θ_{ij} is the opening angle between particles i and j. Up to power-suppressed effects in R_0, the results of this paper can

be extended to non-zero rapidity ($y \neq 0$) by simply replacing θ_{ij} with the rapidity-azimuth distance R_{ij} and the energy fraction z_i with the momentum fraction $p_{Ti}/p_{T\text{jet}}$.

3.1 Leading-Order Calculation

We start our analysis with a relatively simple calculation, by computing the leading order (LO) contribution to the $C_1^{(\alpha)}$ distribution in the collinear limit. This limit is appropriate for the small R_0 assumption considered throughout this paper.

At LO, the jet consists of only two partons at an angular distance $\Delta R_{12} \simeq \theta$, which carry fractions z and $(1-z)$ of the jet's energy. To have a non-zero contribution to $C_1^{(\alpha)}$, both partons must pass the soft-drop condition. In the collinear limit, the groomed $C_1^{(\alpha)}$ distribution is

$$
\frac{1}{\sigma}\frac{d\sigma^{\text{LO}}}{dC_1^{(\alpha)}} = \frac{\alpha_s}{\pi}\int_0^{R_0}\frac{d\theta}{\theta}\int_0^1 dz\, p_i(z)\,\Theta\left(z - z_{\text{cut}}\left(\frac{\theta}{R_0}\right)^\beta\right)\Theta\left(1 - z - z_{\text{cut}}\left(\frac{\theta}{R_0}\right)^\beta\right)
$$
$$
\times\,\delta\left(C_1^{(\alpha)} - z(1-z)\left(\frac{\theta}{R_0}\right)^\alpha\right), \quad (3.4)
$$

where $p_i(z)$ is the appropriate splitting function for a quark-initiated jet ($i = q$) or a gluon-initiated jet ($i = g$), as defined in Eq. (A.4). The two theta functions impose the soft drop condition, and the delta function implements the $C_1^{(\alpha)}$ measurement.

Because we work in the limit where $C_1^{(\alpha)} \ll z_{\text{cut}} \ll 1$, we can ignore terms suppressed by powers of z_{cut} (but we do not need to resum logarithms of z_{cut}); this implies that we can ignore the second theta function in Eq. (3.4). Only focusing on the logarithmically-enhanced contributions, we can also drop the factor of $(1-z)$ in the delta function. These simplifications lead to

$$
\frac{1}{\sigma}\frac{d\sigma^{\text{LO}}}{dC_1^{(\alpha)}} \simeq \frac{\alpha_s}{\pi}\int_0^{R_0}\frac{d\theta}{\theta}\int_0^1 dz\, p_i(z)\,\Theta\left(z - z_{\text{cut}}\left(\frac{\theta}{R_0}\right)^\beta\right)\delta\left(C_1^{(\alpha)} - z\left(\frac{\theta}{R_0}\right)^\alpha\right). \quad (3.5)
$$

For $\beta \geq 0$, the evaluation of the two integrals is straightforward:

$$
\beta \geq 0: \quad \frac{C_1^{(\alpha)}}{\sigma}\frac{d\sigma^{\text{LO}}}{dC_1^{(\alpha)}} \simeq \frac{\alpha_s C_i}{\pi}\frac{2}{\alpha}\times\begin{cases}\log\frac{1}{C_1^{(\alpha)}} + B_i, & C_1^{(\alpha)} > z_{\text{cut}},\\[2mm]\frac{\beta}{\alpha+\beta}\log\frac{1}{C_1^{(\alpha)}} + \frac{\alpha}{\alpha+\beta}\log\frac{1}{z_{\text{cut}}} + B_i, & C_1^{(\alpha)} < z_{\text{cut}},\end{cases} \quad (3.6)
$$

up to terms that are power-suppressed in $C_1^{(\alpha)}$ or z_{cut}. Here, C_i is the overall color factor for the jet ($C_q = C_F = 4/3$ for quarks and $C_g = C_A = 3$ for gluons) and B_i originates from hard-collinear emissions ($B_q = -3/4$ for quarks and $B_g = -\frac{11}{12} + \frac{n_f}{6C_A}$ for gluons, where n_f is the number of active quark flavors). For $\beta < 0$, there is an additional restriction which imposes a minimum allowed value for the observable

$$
\beta < 0: \quad \text{Same as Eq. (3.6) with additional cut } C_1^{(\alpha)} > z_{\text{cut}}^{\alpha/|\beta|}. \quad (3.7)
$$

As often happens for grooming and tagging algorithms [59, 60], the $C_1^{(\alpha)}$ distribution exhibits a transition point at $C_1^{(\alpha)} = z_{\text{cut}}$. Unlike trimming and pruning, though, soft-drop energy correlation functions do not exhibit further (perturbative) transition points at lower values of the observable. For $C_1^{(\alpha)} > z_{\text{cut}}$, soft drop is not active and we recover the ungroomed result. For $C_1^{(\alpha)} < z_{\text{cut}}$, soft drop is active and jets that fail the soft drop condition are either removed from consideration (tagging mode) or assigned $C_1^{(\alpha)} = 0$ (grooming mode). Note that for $\beta > 0$, the logarithmic structure of Eq. (3.6) is of the same order on both sides of the transition point, so the overall cumulative distribution exhibits Sudakov double logarithms. The effect of the soft drop procedure is to reduce the coefficient of the double logarithm by a factor of $\beta/(\alpha + \beta)$.

It is instructive to take different limits of the result in Eq. (3.6). Consider the $\beta \to \infty$ limit at fixed α and z_{cut}. This limit should correspond to no grooming, and indeed, in this limit, we recover the expected LO result for the energy correlation function of the ungroomed jet. Now consider the case $\beta = 0$, which should correspond to the mMDT limit. This limit kills the logarithmic contribution for $C_1^{(\alpha)} < z_{\text{cut}}$, which results in a cumulative distribution that only has single logarithms in $C_1^{(\alpha)}$. This result is the generalization to $C_1^{(\alpha)}$ of the fact that the mMDT jet mass distribution (here $\alpha = 2$) is only single logarithmic [59, 60].

3.2 Modified Leading Logarithmic Approximation

Because of the potentially large logarithms $L \equiv \log(1/C_1^{(\alpha)})$ in Eq. (3.6), we need to perform some kind of resummation in order to get realistic predictions for the $C_1^{(\alpha)}$ distribution. Here, we investigate a simple approximation to the all-order $C_1^{(\alpha)}$ distribution by working to modified leading logarithmic (MLL) accuracy, i.e. we aim to capture the terms $\alpha_s^n L^{2n-q}$ with $q = 0, 1$ in the expansion of the cumulative distribution $\Sigma(C_1^{(\alpha)})$, which gives the probability for the observable to be less than a given value $C_1^{(\alpha)}$.

To MLL order, we need to consider the independent emission of any number of soft or collinear gluons within a jet, with the scale of the (one-loop) coupling chosen at the relative transverse momentum scale κ of the splitting. In the collinear approximation used throughout this paper, we have $\kappa = z\,\theta\,p_{T\text{jet}}$ for jets at arbitrary rapidity.

Virtual emissions are associated with $C_1^{(\alpha)} = 0$ and therefore always contribute to $\Sigma(C_1^{(\alpha)})$. A real emission contributes to $\Sigma(C_1^{(\alpha)})$ either if it has been groomed away or if it lies at an angle smaller than the first emission that passes the soft drop condition. This is illustrated in Fig. 2. Note that the dominant emission contributing to the value of $C_1^{(\alpha)}$ must always lie at an angle less than or equal to the angle of the first emission that passes the soft drop condition, so we do not need to consider the correlation of the groomed jet radius and the value of $C_1^{(\alpha)}$.

The details of the MLL calculation and explicit results are presented in App. A. After one explicitly does the sum over all included real emissions, the cumulative distribution can be interpreted in terms of the phase space for vetoed real emissions. This gives the Sudakov
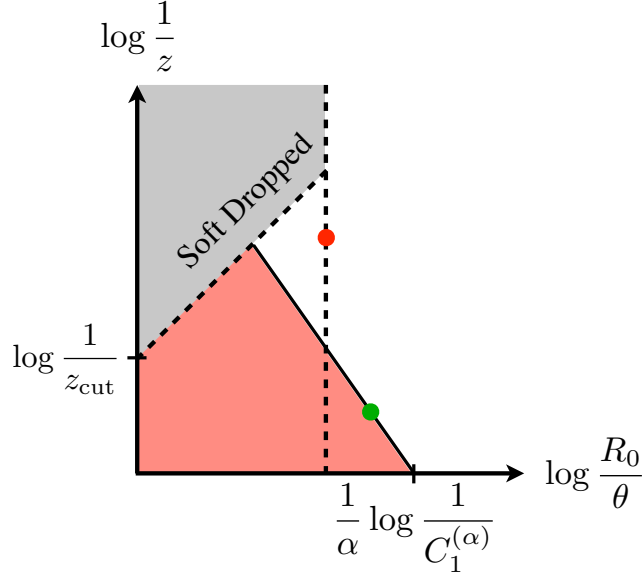
Figure 2: Phase space for emissions relevant for $C_1^{(\alpha)}$ in the $(\log \frac{1}{z}, \log \frac{R_0}{\theta})$ plane. The soft dropped region is gray and the first emission satisfying the soft drop criteria is illustrated by the red dot. The leading emission for $C_1^{(\alpha)}$ is illustrated by the green dot with the forbidden emission region (the Sudakov exponent) shaded in pink.

exponent

$$\Sigma(C_1^{(\alpha)}) = \exp\left[-\frac{1}{\alpha}\int_{C_1^{(\alpha)}}^1 \frac{dc}{c} \int_{\max\left(c,\, z_{\text{cut}}^{\frac{\alpha}{\alpha+\beta}} c^{\frac{\beta}{\alpha+\beta}}\right)}^1 dz\, p_i(z) \frac{\alpha_s(\kappa)}{\pi}\right]\,, \qquad (3.8)$$

where we have introduced the convenient change of variables $c = z\left(\frac{\theta}{R_0}\right)^\alpha$. The integral in the exponent corresponds to real emissions that are not removed by the soft drop procedure, but would give a too large contribution to $C_1^{(\alpha)}$ (corresponding to the pink shaded region in Fig. 2). As expected, the $\beta \to \infty$ limit corresponds to the ungroomed result, and the $\beta = 0$ (mMDT) limit matches the jet mass ($\alpha = 2$) distribution in Ref. [59].

To better understand the logarithmic structure of the soft-dropped energy correlation functions, it is instructive to perform the integrals in Eq. (3.8) in a fixed coupling approximation. For $\beta \geq 0$, neglecting power-suppressed terms, we obtain

$$\Sigma(C_1^{(\alpha)}) \stackrel{\text{f.c.}}{=} \exp\left\{ -\frac{\alpha_s C_i}{\pi}\frac{2}{\alpha}\left[\left(\frac{1}{2}\log^2\frac{1}{C_1^{(\alpha)}} + B_i\log\frac{1}{C_1^{(\alpha)}}\right)\Theta\left(1 - C_1^{(\alpha)}\right)\Theta\left(C_1^{(\alpha)} - z_{\text{cut}}\right)\right.\right.$$

$$+ \left(\frac{\beta}{2(\alpha+\beta)}\log^2\frac{1}{C_1^{(\alpha)}} + \frac{\alpha}{\alpha+\beta}\log\frac{1}{z_{\text{cut}}}\log\frac{1}{C_1^{(\alpha)}} - \frac{\alpha}{2(\alpha+\beta)}\log^2\frac{1}{z_{\text{cut}}} + B_i\log\frac{1}{C_1^{(\alpha)}}\right)$$

$$\left.\left. \times \Theta\left(z_{\text{cut}} - C_1^{(\alpha)}\right)\right]\right\}, \quad (3.9)$$

which is the exponential of the cumulative distribution at LO (i.e. the integral of Eq. (3.6)). For $\beta < 0$, we find an expression analogous to Eq. (3.9), but with a lower bound which enforces $C_1^{(\alpha)} > z_{\text{cut}}^{\alpha/|\beta|}$, thus regulating the soft-collinear behavior. The limiting values of Eq. (3.9) behave as expected. For $\beta \to \infty$, the regions above and below z_{cut} give identical results, so they can be combined to return the ungroomed distribution. For $\beta = 0$, the coefficient of the double logarithm in the region $C_1^{(\alpha)} < z_{\text{cut}}$ vanishes and we obtain the expected mMDT single logarithmic result.

3.3 Multiple Emissions

Multiple gluon emissions within a jet can affect the value of $C_1^{(\alpha)}$. While this effect is strictly speaking beyond MLL accuracy, it is an important component of a full NLL calculation, so it is worth considering how they might affect the $C_1^{(\alpha)}$ distribution. For multiple emissions, we need to determine what region of phase space can have several emissions that contribute to the measured value of the observable. To logarithmic accuracy, these emissions must give comparable contributions to the final measured value of the observable.

For the case of the energy correlation function $C_1^{(\alpha)}$, the region of phase space where multiple emissions contribute can be seen in Fig. 2. For the green emission that sets the value of $C_1^{(\alpha)}$, multiple emissions that contribute logarithmically must lie near the diagonal line defining a fixed value for $C_1^{(\alpha)}$. Everywhere along this diagonal line satisfies the soft drop groomer, and therefore all emissions that contribute to the value of $C_1^{(\alpha)}$ pass the soft drop phase space requirements.[4] Also, because C/A clustering enforces angular ordering, these multiple emissions must lie at angles smaller than the first emission that passes the soft drop requirement. Therefore, accounting for multiple emissions requires including an arbitrary number of emissions that contribute to $C_1^{(\alpha)}$ and pass the soft drop requirement.

To single logarithmic accuracy, the cumulative distribution of soft drop groomed $C_1^{(\alpha)}$ can then be expressed as an explicit sum over uncorrelated emissions as

$$\Sigma(C_1^{(\alpha)}) = \sum_{n=1}^{\infty}\prod_{m=1}^{n}\left[\int_0^{R_0}\frac{d\theta_m}{\theta_m}\int_0^1 dz_m\, p_i(z_m)\frac{\alpha_s(\kappa_m)}{\pi}\Theta\left(z_m - z_{\text{cut}}\left(\frac{\theta_m}{R_0}\right)^\beta\right)\Theta\left(\theta_{i-1} - \theta_i\right)\right]$$

---

[4] One might worry that if the emission that sets the value of $C_1^{(\alpha)}$ lies near the boundary between the soft-drop groomed region and soft-drop kept region, then emissions that contribute to the observable may not satisfy the soft-drop requirement on their own. While this is true, the contributions from such emissions are subleading to the accuracy to which we work and can therefore be ignored.

$$\times \, \Theta \left(C_1^{(\alpha)} - \sum_{m=1}^{n} z_m \left(\frac{\theta_m}{R_0} \right)^\alpha \right) e^{-\int_0^{R_0} \frac{d\theta}{\theta} \int_0^1 dz \, p_i(z) \frac{\alpha_s(\kappa)}{\pi} \Theta \left(z - z_{\text{cut}} \left(\frac{\theta}{R_0} \right)^\beta \right)} \, . \qquad (3.10)$$

The requirement $\Theta \left(\theta_{i-1} - \theta_i \right)$ imposes angular ordering and the explicit exponential is the sum of virtual contributions. The explicit sum can be evaluated by a Laplace transformation which yields

$$\Sigma(C_1^{(\alpha)}) = \int \frac{d\nu}{2\pi i \nu} \, e^{\nu C_1^{(\alpha)}} e^{-R\left(\nu^{-1} \right)} \, , \qquad (3.11)$$

where the ν integral represents the inverse Laplace transform. The function $R(\nu^{-1})$ is called the radiator and is

$$R \left(\nu^{-1} \right) = \int_0^{R_0} \frac{d\theta}{\theta} \int_0^1 dz \, p(z) \frac{\alpha_s(\kappa)}{\pi} \Theta \left(z - z_{\text{cut}} \left(\frac{\theta}{R_0} \right)^\beta \right) \left(1 - \exp \left[-\nu z \left(\frac{\theta}{R_0} \right)^\alpha \right] \right) \, . \qquad (3.12)$$

Because they are Laplace conjugates of one another, logarithmic accuracy in $C_1^{(\alpha)}$ corresponds to the same logarithmic accuracy in ν. Therefore, for single logarithmic accuracy in $C_1^{(\alpha)}$, we must compute the radiator to single logarithmic accuracy in ν. Expanding around $\nu^{-1} = C_1^{(\alpha)}$, the inverse Laplace transform can be evaluated explicitly (see e.g. Ref. [114–116]) and we find

$$\Sigma(C_1^{(\alpha)}) = \frac{e^{-\gamma_E R'(C_1^{(\alpha)})}}{\Gamma \left(1 + R'(C_1^{(\alpha)}) \right)} e^{-R(C_1^{(\alpha)})} \, , \qquad (3.13)$$

where

$$R(C_1^{(\alpha)}) = \int_0^{R_0} \frac{d\theta}{\theta} \int_0^1 dz \, p(z) \frac{\alpha_s(\kappa)}{\pi} \Theta \left(z - z_{\text{cut}} \left(\frac{\theta}{R_0} \right)^\beta \right) \Theta \left(z \left(\frac{\theta}{R_0} \right)^\alpha - C_1^{(\alpha)} \right) \, , \qquad (3.14)$$

γ_E is the Euler-Mascheroni constant, Γ is the gamma function, and

$$R'(C_1^{(\alpha)}) = -\frac{\partial}{\partial \log C_1^{(\alpha)}} R(C_1^{(\alpha)}) \, . \qquad (3.15)$$

The prefactor in Eq. (3.13) containing $R'(C_1^{(\alpha)})$ captures the effect of multiple emissions on the distribution of $C_1^{(\alpha)}$. We remind the reader that to single-logarithmic accuracy, we can neglect the hard-collinear contribution in the multiple-emission prefactor, i.e. we can take $B_i = 0$ in Eq. (3.15).

Multiple-emission contributions to the ungroomed $C_1^{(\alpha)}$ distribution were considered in Ref. [44]. The effect is non-negligible for the jet-mass like case ($\alpha = 2$) and increases as α grows smaller. However, we expect these kind of contributions to be reduced by the soft-drop procedure, essentially because the coefficient of the soft-collinear terms, which give the single-logarithmic contribution to R', is reduced by a factor $\mathcal{O}(\beta)$. We shall come back to this discussion in Sec. 3.5, when we compare the resummed calculation to a result obtained with a parton shower event generator.

The differential distribution for the observable $C_1^{(\alpha)}$ with multiple emissions, i.e. the derivative of Eq. (3.13), depends on the second derivative of the radiator function R. However, within our approximations, R'' is not continuous across $C_1^{(\alpha)} = z_{\text{cut}}$ (see for instance Eq. (3.9)). Physically, this is a consequence of the fact that emissions that contribute similarly to the observable can occur on either side of the z_{cut} transition point. As a result, the distribution with multiple emission exhibits a discontinuity at $C_1^{(\alpha)} = z_{\text{cut}}$ because of terms which are beyond NLL accuracy in $\log \Sigma$. In order to restore continuity, we can simply replace the logarithmic derivative with its discrete version:

$$R'(C_1^{(\alpha)}) \to \frac{R(C_1^{(\alpha)} e^{-\delta}) - R(C_1^{(\alpha)})}{\delta} \ . \tag{3.16}$$

The specific choice of δ is irrelevant to single logarithmic accuracy, and we take $\delta = 1$ for definiteness. One can think of the δ-dependence as being one source of theoretical uncertainty.

3.4 Non-Global Logarithms

The jet-based $C_1^{(\alpha)}$ is an example of a non-global observable [104], meaning that it receives single-logarithmic contributions coming from an ensemble of gluons that are outside of the jet which then radiate soft gluons into the jet. The resummation of non-global logarithms for the specific case of the mass of anti-k_t jets ($\alpha = 2$) was performed in Refs. [92, 93] in the large N_C limit (for recent work at finite N_C see Ref. [117]). A key result of Refs. [59, 60] is that the mass distribution of an mMDT jet is free of non-global logarithms, since the mMDT eliminates all sensitivity to soft emissions. Since non-global logarithms contribute only at the single-logarithmic level, they are formally beyond MLL accuracy. That said, it is interesting to study the structure of non-global logarithms for soft-dropped $C_1^{(\alpha)}$ as β is varied, especially since we know non-global logarithms must vanish at $\beta = 0$.

Consider the lowest-order configuration that can produce a non-global logarithm, namely the correlated emission of two gluons where k_1 is outside the original anti-k_t jet and a softer gluon k_2 is inside it.[5] To contribute to a non-global logarithm, k_2 has to pass the soft-drop condition, so the relevant phase space constraints are

$$\Theta^{\text{NG}} \equiv \Theta\left(z_1 - z_2\right) \Theta\left(\theta_1 - R_0\right) \Theta\left(R_0 - \theta_2\right) \Theta\left(z_2 - z_{\text{cut}}\left(\frac{\theta_2}{R_0}\right)^\beta\right). \tag{3.17}$$

To extract the non-global contribution, we have consider the $C_F C_A$ correlated emission term of the squared matrix element for two gluon emissions that satisfy the Θ^{NG} constraint:

$$\frac{1}{\sigma}\frac{d\sigma^{\text{NG}}}{dC_1^{(\alpha)}} = 4C_F C_A \left(\frac{\alpha_s}{2\pi}\right)^2 \int \frac{dz_1}{z_1}\frac{dz_2}{z_2} \int \theta_2 d\theta_2 \int \theta_1 d\theta_1 \, \Omega_2 \, \Theta^{\text{NG}} \delta\left(C_1^{(\alpha)} - z_2\left(\frac{\theta_2}{R_0}\right)^\alpha\right), \tag{3.18}$$

where Ω_2 is the (azimuthally averaged) angular function (see for example [119])

$$\Omega_2 = \frac{2}{(1 - \cos\theta_1)(1 + \cos\theta_2)|\cos\theta_1 - \cos\theta_2|} \simeq \frac{4}{\theta_1^2(\theta_1^2 - \theta_2^2)}. \tag{3.19}$$

---

[5]Because the original jet is defined with the anti-k_t algorithm, we are not sensitive to clustering logarithms first described in Ref. [118].

It is now relatively easy to evaluate Eq. (3.18). For definiteness, we consider $\beta \geq 0$ and obtain

$$
\frac{C_1^{(\alpha)}}{\sigma} \frac{d\sigma^{\mathrm{NG}}}{dC_1^{(\alpha)}} = 4 C_F C_A \left(\frac{\alpha_s}{2\pi}\right)^2 \int_{R_0^2}^1 d\theta_1^2 \int_0^{R_0^2} d\theta_2^2 \, \Theta\left(\theta_2^\alpha - R_0^\alpha C_1^{(\alpha)}\right) \Theta\left(R_0 \left(\frac{C_1^{(\alpha)}}{z_{\mathrm{cut}}}\right)^{\frac{1}{\alpha+\beta}} - \theta_2\right)
$$

$$
\times \frac{1}{\theta_1^2(\theta_1^2 - \theta_2^2)} \log \frac{\theta_2^\alpha}{R_0^\alpha C_1^{(\alpha)}}
$$

$$
= 4 C_F C_A \left(\frac{\alpha_s}{2\pi}\right)^2 \left[\mathrm{Li}_2\left(\left(\frac{C_1^{(\alpha)}}{z_{\mathrm{cut}}}\right)^{\frac{2}{\alpha+\beta}}\right) \frac{\alpha \log \frac{1}{z_{\mathrm{cut}}} + \beta \log \frac{1}{C_1^{(\alpha)}}}{\alpha + \beta} \right.
$$

$$
\left. + \frac{\alpha}{2} \mathrm{Li}_3\left(C_1^{(\alpha)\frac{2}{\alpha}}\right) - \frac{\alpha}{2} \mathrm{Li}_3\left(\left(\frac{C_1^{(\alpha)}}{z_{\mathrm{cut}}}\right)^{\frac{2}{\alpha+\beta}}\right) \right] + \mathcal{O}(R_0^2). \quad (3.20)
$$

By itself, Eq. (3.20) is not particularly enlightening, so it is instructive to take the no grooming limit ($\beta \to \infty$) and the mMDT limit ($\beta = 0$). To get a sensible result, we first take the limit of Eq. (3.20) with respect to β and then consider the behavior of the resulting expression at small $C_1^{(\alpha)}$. For $\beta \to \infty$,

$$
\lim_{\beta \to \infty} \frac{C_1^{(\alpha)}}{\sigma} \frac{d\sigma^{\mathrm{NG}}}{dC_1^{(\alpha)}} = C_F C_A \left(\frac{\alpha_s}{2\pi}\right)^2 \left(\frac{2}{3}\pi^2 \log \frac{1}{C_1^{(\alpha)}} + \cdots\right) + \mathcal{O}(\beta^{-1}), \quad (3.21)
$$

where the dots indicate terms that are not logarithmically enhanced at small $C_1^{(\alpha)}$. Eq. (3.21) is precisely the result for anti-k_t jets in the small jet radius limit [92], and extends to all $\alpha > 0$ since the non-global logarithms arise from soft wide-angle emissions for which the specific angular exponent is a power correction.

For $\beta = 0$, there are no non-global logarithms. In particular, the $\log C_1^{(\alpha)}$ term in Eq. (3.20) has null coefficient and, after taking the small $C_1^{(\alpha)}$ limit, we obtain

$$
\lim_{\beta \to 0} \frac{C_1^{(\alpha)}}{\sigma} \frac{d\sigma^{\mathrm{NG}}}{dC_1^{(\alpha)}} = C_F C_A \left(\frac{\alpha_s}{2\pi}\right)^2 \left(\frac{C_1^{(\alpha)}}{z_{\mathrm{cut}}}\right)^{\frac{2}{\alpha}} \left(4 \log \frac{1}{z_{\mathrm{cut}}} - 2\alpha\left(1 - z_{\mathrm{cut}}^{\frac{2}{\alpha}}\right) + \cdots\right) + \mathcal{O}(\beta).
$$
$$(3.22)$$

This expression is consistent with the small-z_{cut} and small-R_0 limit of result for the mMDT mass distribution ($\alpha = 2$) [60].

In general, for finite values of $\beta > 0$, the non-global logarithms are suppressed by powers of $C_1^{(\alpha)}$ with respect to the anti-k_t ($\beta \to \infty$) case. Taking the small $C_1^{(\alpha)}$ limit of Eq. (3.20), we find[6]

$$
\lim_{C_1^{(\alpha)} \to 0} \frac{C_1^{(\alpha)}}{\sigma} \frac{d\sigma^{\mathrm{NG}}}{dC_1^{(\alpha)}} = 4 C_F C_A \left(\frac{\alpha_s}{2\pi}\right)^2 \frac{\beta}{\alpha+\beta} \left(\frac{C_1^{(\alpha)}}{z_{\mathrm{cut}}}\right)^{\frac{2}{\alpha+\beta}} \log \frac{1}{C_1^{(\alpha)}} + \mathcal{O}\left(C_1^{(\alpha)\frac{2}{\alpha+\beta}}\right). \quad (3.23)
$$

---

[6]Note that the limits $\beta \to \infty$ and $C_1^{(\alpha)} \to 0$ do not commute with one another as Eq. (3.21) does not follow from the $\beta \to \infty$ limit of Eq. (3.23).

Because the non-global logarithms are formally power suppressed, we can consistently neglect their resummation to NLL accuracy. As expected, soft drop declustering removes soft divergences, and hence removes non-global logarithms.

3.5   Comparison to Monte Carlo

We conclude our discussion of $C_1^{(\alpha)}$ by comparing our analytic MLL calculation in Sec. 3.2 (plus the multiple-emission corrections from Sec. 3.3) to a standard Monte Carlo parton shower. For these simulations, we use PYTHIA 8.175 [120] (p_t-ordered shower) with the default 4C tune [121]. We consider proton-proton collisions at 14 TeV at parton level, including initial- and final-state showering but without multiple parton interactions (i.e. UE). We discuss UE and hadronization corrections in Sec. 6.

Jets clustering is performed with the anti-k_t algorithm [109] with radius $R_0 = 1.0$ [7] using a development version of FASTJET 3.1 (which for the features used here behaves identically to the 3.0.x series [123]). A transverse momentum selection cut $p_T > 3$ TeV is applied on the jets before grooming. To implement the soft drop procedure described in Sec. 2, jets are reclustered using exclusive C/A [110, 111] to return the same jet. The soft drop code will be made available as part of the FASTJET contrib project (http://fastjet.hepforge.org/contrib/).

We start by considering the case $\alpha = 2$, which corresponds to the familiar case of the jet mass distribution. In Fig. 3 we show results for $qq \to qq$ scattering for different values of angular power β in the soft-drop declustering procedure ($\beta = 0$ is the mMDT already studied in Ref. [59]). The plot on the left has been obtained from PYTHIA 8, while the one on the right has been obtained with the analytic resummation, evaluated numerically by freezing the strong coupling in the infrared (see App. A). Dashed curves correspond to MLL accuracy Eq. (3.8), while solid ones include the multiple-emission effect from Eq. (3.13).

The plain jet mass case ($\beta \to \infty$, shown in black) exhibits the characteristic Sudakov peak. All the other curves exhibit a transition point at $C_1^{(\alpha)} = z_{\rm cut}$ and soft drop is active for $C_1^{(\alpha)} < z_{\rm cut}$. Soft-dropped distributions with $\beta > 0$ (blue and red) are double logarithmic and indeed we can recognize this behavior in the shape of the distribution (i.e. an upside-down parabola on a log-linear plot). The case $\beta = 0$ (mMDT, green) has no soft logarithms, so the resulting distribution is single logarithmic. The distribution is nearly flat because the choice $z_{\rm cut} = 0.1$ is close to the value that minimizes higher-order corrections for quark-initiated jets [59]. As discussed in Eq. (3.7), the choice of negative β (here $\beta = -0.5$ in pink) leads to a distribution with a minimum allowed value, thus regulating both soft and collinear divergencies.

For the groomed distributions, there is good agreement between the parton shower and our analytics. Moreover, we also note that the impact of multiple emissions, i.e. the difference between solid and dashed curves in Fig. 3b, decreases with β. It is perhaps surprising that we

---

[7]We choose $R_0 = 1.0$ primarily to ease the comparison with previous studies of mMDT in Ref. [59]. While we take the small jet radius approximation in this paper, it is known to be reasonable even up to $R_0 \sim 1$ [93, 122].
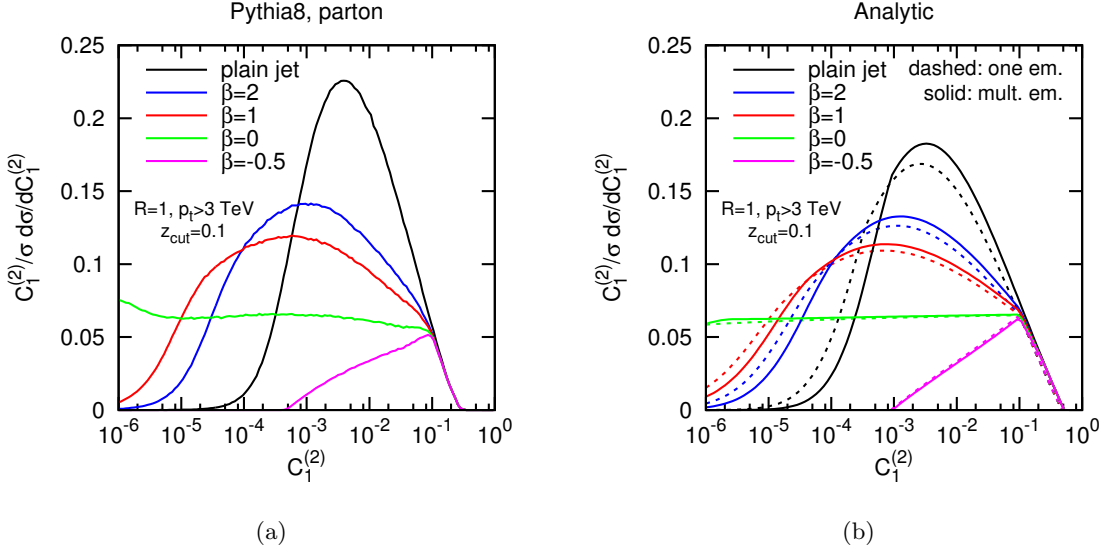
Figure 3: The energy correlation functions $C_1^{(\alpha=2)}$ for quark-initiated jets. Here we compare PYTHIA 8 [120] (left), our MLL formula in Eq. (3.8) (right, dashed curves), and our MLL plus multiple-emissions formula in Eq. (3.13) (right, solid curves). These $\alpha = 2$ curves correspond to the case of jet mass-squared (normalized to jet energy squared). We show both the ungroomed (plain jet) distribution, as well as groomed distributions from soft drop declustering with $z_{\text{cut}} = 0.1$ and various values of β. For $\beta = 2, 1$, we see the expected Sudakov double logarithmic peaks, while $\beta = 0$ (mMDT) has only single logarithms and $\beta = -1$ cuts off at small values. The PYTHIA 8 distributions do not have hadronization effects, and the MLL distributions are evaluated by freezing α_s in the infrared.

find worst agreement between analytics and Monte Carlo in the ungroomed (plain jet) case. However, one should keep in mind that although the two approximations are roughly of the same accuracy (MLL), Monte Carlo parton showers also partially contain many subleading effects. Using the results of Refs. [92, 93], we have checked that subleading effects (like initial-state radiation and non-global logarithms) play a non-negligible role. Indeed, PYTHIA 8 is closer to the full NLL result than to the (less accurate) MLL plus multiple emissions one presented here. Because the action of soft drop is to remove large-angle soft radiation (e.g. initial state radiation and non-global logarithms), it is reassuring that our calculations for the finite β soft-drop curves are indeed in better agreement with the parton shower.

In Fig. 4, we compare our analytic resummation to the parton shower for $C_1^{(\alpha)}$ with $\alpha = 1.5, 1, 0.5$. Again, the plots on the left are obtained with PYTHIA 8 while the ones on the right are the MLL plus multiple emissions results. The same gross features seen with $\alpha = 2$ are also present here, including the fact that the agreement between Monte Carlo and analytics is better with grooming than without. Overall, however, the agreement gets worse
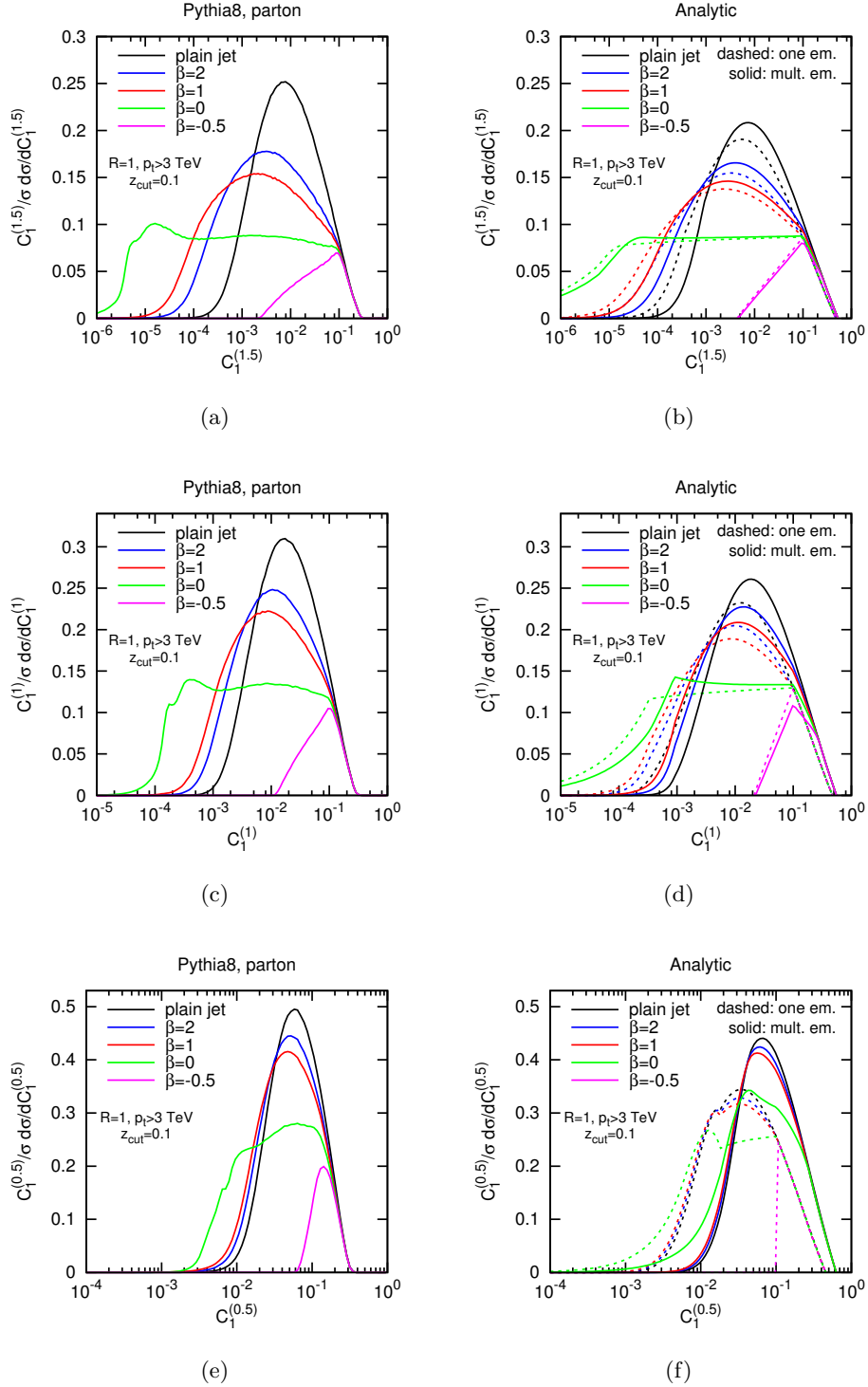
Figure 4: The energy correlation functions $C_1^{(\alpha)}$ with $\alpha = 1.5, 1, 0.5$ (top to bottom) for quark-initiated jets. The plots on the left are obtained with PYTHIA 8, while the ones of the right are our MLL predictions (dashed) with multiple emissions included (solid).

as α decreases. This is likely because, as seen in Eq. (3.6), the expansion parameter is really α_s/α, so both logarithmically-enhanced and non-singular fixed-order corrections are more important at small α. It is encouraging that the peak locations are still roughly the same in the analytic calculations and PYTHIA 8 results, even if the overall peak normalizations slightly differ. We note that the dashed curves in Fig. 4f have kinks; indeed all the curves in this section obtained from analytic calculations suffer from the same behavior, although this feature is not visible on the other plots. The position of the kink is $C_1^{(\alpha)} = \left(\frac{\mu_{\mathrm{NP}}}{p_T R_0}\right)^\alpha$ and it is a consequence of the way we freeze the running coupling at $\kappa = \mu_{\mathrm{NP}}$. As detailed in App. A, this effect is beyond the accuracy of our calculation. Finally, in Figs. 4e and 4f, note the sharp cutoff of the plots when $\alpha + \beta = 0$, which can be understood from Eq. (3.7). In Fig. 4f, we only show the MLL result since fixed-order corrections are expected to be important and our treatment of multiple emissions effects in Eq. (3.16) becomes singular when $\alpha + \beta = 0$.

4 Groomed Jet Radius

Because the soft drop procedure is defined through declustering a C/A branching tree, there is a well-defined and IRC-safe meaning to the groomed jet radius. Concretely, the groomed jet radius R_g is the angle between the branches that first satisfy Eq. (1.1), which is sensible because for a C/A tree, all subsequent branches are separated by an angle less than R_g. From a practical perspective, R_g is particularly interesting, since the groomed jet area is approximately πR_g^2. Thus, R_g serves as a proxy for the sensitivity of the groomed jet to possible contamination from pileup [124, 125].

4.1 Modified Leading Logarithmic Approximation

The calculation of the groomed jet radius to MLL accuracy follows much of the same logic as the $C_1^{(\alpha)}$ calculation in Sec. 3.2. As illustrated in Fig. 5, R_g actually corresponds to a simpler phase space than $C_1^{(\alpha)}$. A given value of R_g simply means that all emissions at angles larger than R_g failed the soft drop criteria. Therefore, the R_g distribution can be calculated by demanding that all emissions at angles larger than R_g were groomed away. As explained in more detail in App. B, this understanding translates into the following cumulative distribution for the groomed jet radius:

$$\Sigma^{\mathrm{radius}}(R_g) = \exp\left[-\int_{R_g}^{R_0} \frac{d\theta}{\theta} \int_0^1 dz\, p_i(z)\, \frac{\alpha_s(\kappa)}{\pi} \Theta\left(z - z_{\mathrm{cut}} \frac{\theta^\beta}{R_0^\beta}\right)\right] , \qquad (4.1)$$

where the integral in the exponent again corresponds to vetoed emissions (i.e. the pink region in Fig. 5).

Besides the simpler phase space for one emission, R_g is also simpler than $C_1^{(\alpha)}$ with respect to multiple emissions. In the case of $C_1^{(\alpha)}$, multiple emissions could contribute to the value of $C_1^{(\alpha)}$, but the MLL approximation effectively only considers the contribution from a single dominant emission. For R_g, though, once one emission satisfies the soft drop criteria,
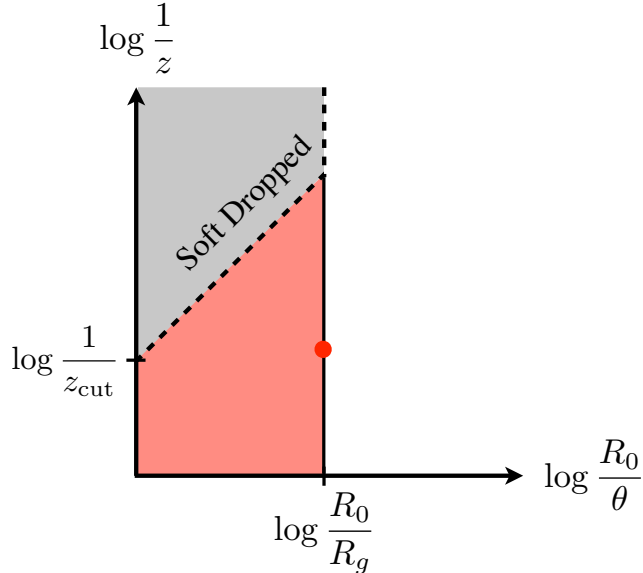
Figure 5: Phase space for emissions relevant for groomed jet radius R_g in the $(\log \frac{1}{z}, \log \frac{R_0}{\theta})$ plane. The soft dropped region is gray and the first emission satisfying the soft drop criteria is illustrated by the red dot. The forbidden emission region (the Sudakov exponent) is shaded in pink.

the jet radius is set, so multiple emissions do not contribute to this observable. We have also verified that non-global contributions are suppressed by R_g for $\beta < \infty$, analogously to the energy correlation case. For these reasons, we believe that the expression in Eq. (4.1) is fully accurate to single-logarithmic level,[8] though for consistency with the rest of this paper, we will only evaluate Eq. (4.1) to MLL accuracy.

4.2 Comparison to Monte Carlo

There are two different ways one can define the groomed jet radius in Monte Carlo. The first method is to simply measure the R_g value of the C/A branching that satisfies the soft drop condition. A second approach, more directly relevant for pileup mitigation, is to determine the effective radius of the groomed jet from its active area [108]. The active area of a jet is defined as the area over which infinitesimally soft particles are clustered into the jet. An effective jet radius R_{eff} can then be defined from the groomed jet active area using:

$$R_{\text{eff}} \equiv \left(\frac{A_{\text{active}}}{\pi \xi} \right)^{1/2} , \tag{4.2}$$

---

[8]Strictly speaking, NLL accuracy requires evaluating the strong coupling at two loops, i.e. with β_1, in the CMW scheme [126].
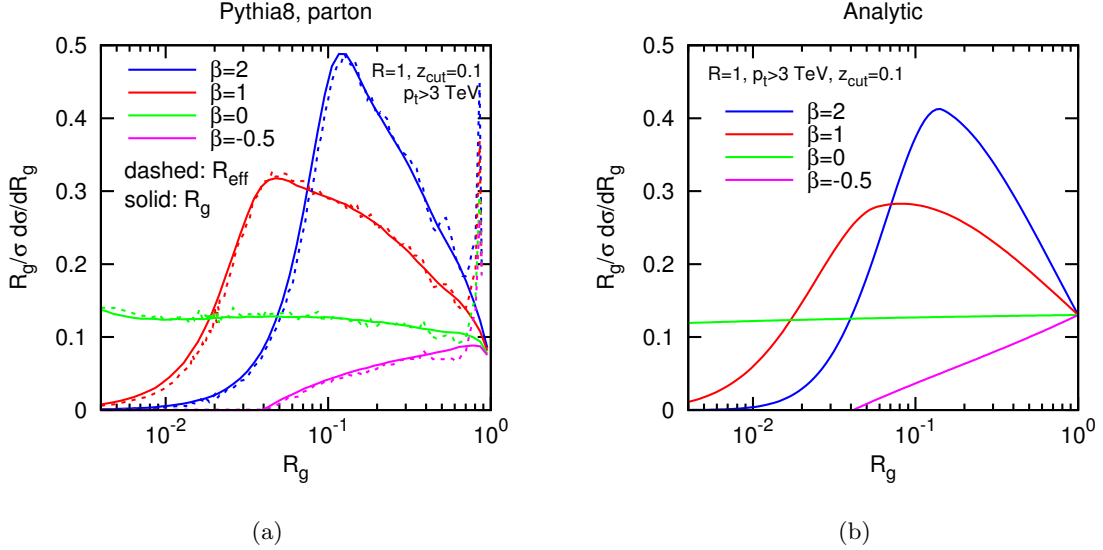
Figure 6: Comparison of the jet radius R_g distribution extracted from PYTHIA 8 (left, solid) and inferred from the active area in PYTHIA 8 using $R_{\text{eff}} = \sqrt{A_{\text{active}}/\pi\xi}$ (left, dashed), and computed to MLL accuracy (right). The original jet radius is set to be $R_0 = 1$ and the jets have an ungroomed energy of 3 TeV. The soft drop parameter is $z_{\text{cut}} = 0.1$, while β is varied.

where A_{active} is the active jet area, and $\xi \simeq (1.16)^2$ accounts for the fact that a typical C/A jet of radius R_0 has an average active area $\xi\pi R_0^2$.[9]

In Fig. 6a we show the R_g and R_{eff} distributions as measured on the same PYTHIA jet samples introduced in Sec. 3.5. To obtain R_{eff} in practice, we have computed the groomed jet area using active areas as implemented in FASTJET (v3), and we used a ghost area of 0.0005 and 10 repetitions in order to reach sufficiently small values of R_{eff}. With the ξ offset factor, the two techniques give remarkably similar results, giving strong evidence that the groomed jet radius R_g is an effective measure of pileup sensitivity. The main difference is the spike at $R_{\text{eff}} = 1/\sqrt{\xi}$, corresponding to cases where the first C/A branching already satisfies the soft drop condition, yet typically with $R_g < 1$. The nice reduction of the jet area even with mild grooming (e.g. $\beta = 2$) suggests that soft drop should work well for pileup mitigation, but we leave a detailed study to future work.

In Fig. 6b, we show the MLL distribution from Eq. (4.1). There is good qualitative agreement with PYTHIA for a range of angular exponents β, suggesting that our MLL calculation for R_g captures the relevant physics effects present in the Monte Carlo simulation.

---

[9]The numerical value for ξ can be read from Fig. 8 in Ref. [108]. Strictly speaking, this result is only valid for a jet made of two particles separated by R_0, with one of them much softer than the other. However, for C/A jets, one expects that this would not vary much for more symmetric two-particle configurations (see e.g. Ref. [125]).
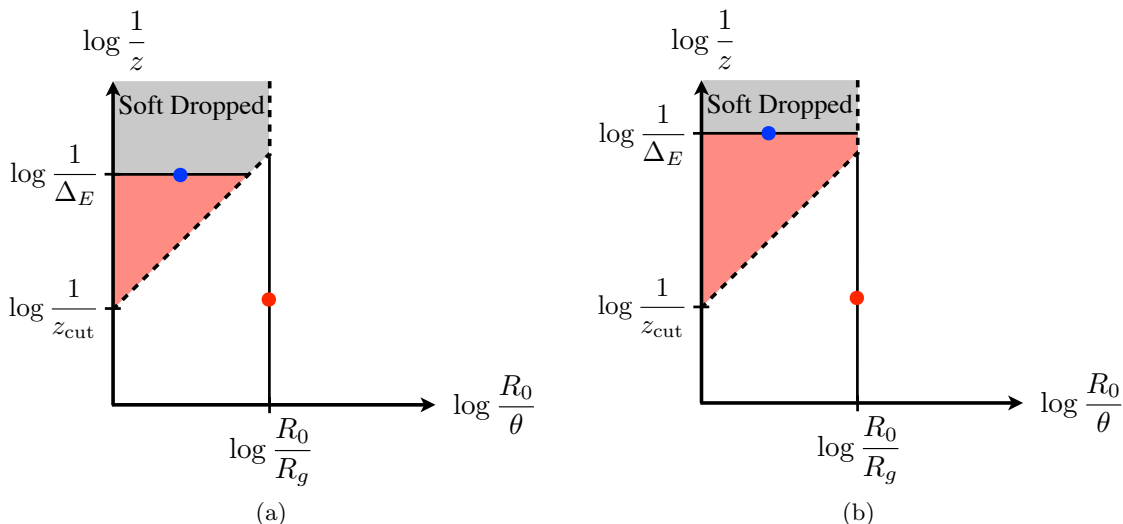
Figure 7: Phase space for emissions relevant for groomed jet energy loss Δ_E in the $(\log \frac{1}{z}, \log \frac{R_0}{\theta})$ plane. The soft dropped region is gray/pink and the first emission satisfying the soft drop criteria is illustrated by the red dot, located at the groomed jet radius, R_g. The blue dot represents the leading contribution to Δ_E, with subleading contributions above it. The location in angle of all soft dropped emissions is larger than R_g. The forbidden emission region for a given value of R_g (the Sudakov exponent) is shaded in pink. The left (right) plot shows Δ_E larger (smaller) than $z_{\text{cut}}(R_g/R_0)^\beta$.

5 Jet Energy Drop

Our final analytic calculation is for the groomed jet energy. Unlike for many other grooming procedures, the energy of a soft-drop jet ($\beta > 0$) is an IRC safe observable and so can be computed in pQCD. In particular, we will study the fractional energy drop due to grooming Δ_E defined as

$$\Delta_E \equiv \frac{E_0 - E_g}{E_0} \ , \tag{5.1}$$

where E_0 is the energy of the jet before grooming and E_g is the energy of the groomed jet. Δ_E can be interpreted as a measure of the fraction of the original jet's energy contained in soft wide-angle emissions. In the small R_0 limit, Δ_E is the same as the fractional p_T loss, which is the more relevant quantity for non-central ($y \neq 0$) jets in hadronic collisions.

5.1 Modified Leading Logarithmic Approximation

At MLL order, the calculation of the Δ_E distribution is more subtle than for $C_1^{(\alpha)}$ or R_g. In the case of $C_1^{(\alpha)}$ and R_g, the Sudakov veto region was effectively determined by a single emission, and the multiple emissions effect for $C_1^{(\alpha)}$ could be included as a higher-order correction (see Sec. 3.3).

For Δ_E, the veto region depends crucially on two emissions, as illustrated in Fig. 7. The energy drop due to grooming comes from large angle emissions that fail the soft drop condition. But to figure out which emissions are dropped, we first have to know which emission satisfied the soft drop condition, since that sets the groomed jet radius R_g. All emissions lying at angles greater than R_g are removed by soft drop, but all emissions at angles less than R_g are maintained. Thus, the energy drop depends both on the emission that sets R_g and on the emissions that contributes to Δ_E.

In practice, the easiest way to determine the Δ_E distribution is by computing the energy drop for a given value of R_g and then integrating over the R_g distribution. In equations, the cumulative distribution of Δ_E is given by

$$\Sigma^{\text{energy-drop}}(\Delta_E) = \int_0^{R_0} dR_g \, \frac{d\Sigma^{\text{radius}}(R_g)}{dR_g} \, \widetilde{\Sigma}(R_g, \Delta_E) \,, \tag{5.2}$$

where $\widetilde{\Sigma}(R_g, \Delta_E)$ is the cumulative distribution of Δ_E for a given groomed jet radius R_g. The cumulative distribution $\Sigma^{\text{radius}}(R_g)$ was defined in Eq. (4.1), and the derivative factor is needed to extract the differential cross section (i.e. the probability distribution) for R_g.

The details of the $\widetilde{\Sigma}(R_g, \Delta_E)$ calculation are presented in App. C. The key is that this double cumulative distribution can be computed at logarithmic accuracy by summing over independent contributions at all orders:

$$\widetilde{\Sigma}(R_g, \Delta_E) = \sum_{n=1}^{\infty} \left[\prod_{m=1}^{n} \int_{R_g}^{R_0} \frac{d\theta_m}{\theta_m} \int_0^1 dz_m \, p_i(z_m) \frac{\alpha_s(\kappa_m)}{\pi} \Theta(\theta_m - \theta_{m+1}) \Theta\left(z_{\text{cut}} \frac{\theta_m^\beta}{R_0^\beta} - z_m \right) \right]$$

$$\times \Theta\left(\Delta_E - \sum_{m=1}^{n} z_m \right) \exp\left[-\int_{R_g}^{R_0} \frac{d\theta}{\theta} \int_0^1 dz \, p_i(z) \frac{\alpha_s(\kappa)}{\pi} \Theta\left(z_{\text{cut}} \frac{\theta^\beta}{R_0^\beta} - z \right) \right]$$

$$= \int \frac{d\nu}{2\pi i \nu} e^{\nu \Delta_E} e^{-R_2\left(R_g, \nu^{-1}\right)} \,. \tag{5.3}$$

Here, we are accounting for the effect of multiple emissions (i.e. the sum over m in the observable) by performing a Laplace transform, and the explicit integral over ν represents the inverse Laplace transform. The radiator function appearing in the exponent is

$$R_2\left(R_g, \nu^{-1}\right) = \int_{R_g}^{R_0} \frac{d\theta}{\theta} \int_0^1 dz \, p_i(z) \frac{\alpha_s(\kappa)}{\pi} \Theta\left(z_{\text{cut}} \frac{\theta^\beta}{R_0^\beta} - z \right) \left(1 - e^{-\nu z} \right) \,, \tag{5.4}$$

which is a function of both the Laplace transform parameter ν and the groomed jet radius R_g.

5.2 Sudakov Safety for $\beta = 0$

As mentioned in Sec. 2.2, the groomed jet energy drop Δ_E is IRC safe only if $\beta > 0$. In particular, the energy of a $\beta = 0$ (mMDT) groomed jet is not an IRC safe quantity, since a measured value of energy does not require two well-separated hard prongs in the jet.

On the other hand, Eq. (5.2) has a smooth $\beta \to 0$ limit, and therefore is still calculable (despite being IRC unsafe). Specifically, we are calculating the Δ_E distribution at a fixed groomed jet radius R_g, which forces a two-prong configuration. There is still an (IRC unsafe) singularity at $R_g \to 0$, but this is regulated by the Sudakov factor in the R_g distribution. This property was referred to as "Sudakov safety" in Ref. [105]. As we will now show, the way in which IRC unsafety but Sudakov safety manifests itself for Δ_E is rather peculiar.

The behavior of Δ_E for $\beta = 0$ is easiest to study by computing the cumulative distribution of the energy drop at fixed coupling. We will also take the Laplace conjugate parameter $\nu \to \infty$ to suppress multiple emissions effects. This limit removes the inverse Laplace transform and turns the exponential factor in Eq. (5.4) into the constraint that $z > \Delta_E$. We emphasize that the $\nu \to \infty$ limit is only taken to simplify the following discussion; the fixed-coupling energy loss distribution with the full multiple emissions effect exhibits the same properties.

At fixed-coupling, the cumulative distribution of the groomed jet radius is

$$
\Sigma^{\text{radius}}(R_g) \overset{\text{f.c.}}{=} \exp\left[-\frac{\alpha_s}{\pi} \int_{R_g}^{R_0} \frac{d\theta}{\theta} \int_{z_{\text{cut}}}^1 dz\, p_i(z)\, \Theta\left(z - z_{\text{cut}} \frac{\theta^\beta}{R_0^\beta} \right) \right]
$$
$$
\simeq \exp\left[-\frac{\alpha_s}{\pi} C_i \left(\beta \log^2 \frac{R_0}{R_g} - 2\log z_{\text{cut}} \log \frac{R_0}{R_g} + 2B_i \log \frac{R_0}{R_g} \right) \right] , \qquad (5.5)
$$

where we have ignored terms suppressed by positive powers of z_{cut} and Δ_E. The cumulative distribution of the energy drop at fixed groomed jet radius is

$$
\widetilde{\Sigma}(R_g, \Delta_E) \overset{\text{f.c.}}{=} \exp\left[-\frac{\alpha_s}{\pi} \int_{R_g}^{R_0} \frac{d\theta}{\theta} \int_{\Delta_E}^{z_{\text{cut}}} dz\, p_i(z)\, \Theta\left(z_{\text{cut}} \frac{\theta^\beta}{R_0^\beta} - z \right) \right]
$$
$$
\simeq \Theta\left(z_{\text{cut}} \frac{R_g^\beta}{R_0^\beta} - \Delta_E \right) \exp\left[-\frac{\alpha_s}{\pi} C_i \left(2\log \frac{z_{\text{cut}}}{\Delta_E} \log \frac{R_0}{R_g} - \beta \log^2 \frac{R_0}{R_g} \right) \right]
$$
$$
+ \Theta\left(\Delta_E - z_{\text{cut}} \frac{R_g^\beta}{R_0^\beta} \right) \Theta(z_{\text{cut}} - \Delta_E) \exp\left[-\frac{\alpha_s}{\pi} \frac{C_i}{\beta} \log^2 \frac{z_{\text{cut}}}{\Delta_E} \right] . \qquad (5.6)
$$

Plugging these expressions into Eq. (5.2) in the $\nu \to \infty$ limit, we find the cumulative distribution of the groomed energy drop to be

$$
\Sigma^{\text{energy-drop}}(\Delta_E) = \frac{\log z_{\text{cut}} - B_i}{\log \Delta_E - B_i} + \frac{\pi\beta}{2C_i\alpha_s(\log \Delta_E - B_i)^2} \left(1 - e^{-2\frac{\alpha_s}{\pi}\frac{C_i}{\beta}\log\frac{z_{\text{cut}}}{\Delta_E}\left(\log\frac{1}{\Delta_E} + B_i \right)} \right) ,
$$
$$
\tag{5.7}
$$

for $\Delta_E < z_{\text{cut}}$. At this order, the cumulative distribution is constant for $\Delta_E > z_{\text{cut}}$.

The expression in Eq. (5.7) has some fascinating properties. First, by expanding order-by-order in α_s, we find

$$
\Sigma^{\text{energy-drop}}(\Delta_E) = 1 - \frac{\alpha_s}{\pi} \frac{C_i}{\beta} \log^2 \frac{z_{\text{cut}}}{\Delta_E} + \mathcal{O}\left(\left(\frac{\alpha_s}{\beta} \right)^2 \right) . \qquad (5.8)
$$

Thus, the expansion in powers of the strong coupling is actually an expansion in α_s/β, which diverges order-by-order in perturbation theory for $\beta \to 0$. Thus, as advertised, the energy drop distribution is not IRC safe for $\beta = 0$. However, the $\beta \to 0$ limit of Eq. (5.7) can be taken before expanding in α_s. The $\beta \to 0$ limit yields the simple and surprising result

$$\Sigma^{\text{energy-drop}}(\Delta_E)_{\beta=0} = \frac{\log z_{\text{cut}} - B_i}{\log \Delta_E - B_i} \ , \tag{5.9}$$

which is completely independent of α_s! So while the strong coupling constant α_s was necessary to calculate Δ_E, the leading behavior is independent of the value of α_s.

We can attribute this behavior to the fact that Δ_E is a Sudakov safe observable for $\beta = 0$. The singular region of phase space at $R_g \to 0$ is exponentially suppressed by the Sudakov factor in $\Sigma^{\text{radius}}(R_g)$. This exponential suppression balances the exponential increase in the number of groomed emissions in such a way that Δ_E is independent of α_s. In fact, Δ_E is independent of the total color of the jet at fixed coupling, and only depends on the flavor of the jet through the subleading terms in the splitting functions B_i. When the running coupling is included, we will see that the dominant contribution to the Δ_E distribution is still independent of α_s, with only weak dependence controlled by the QCD β-function.

5.3 Non-Global Logarithms

The ungroomed jet energy E_0 is clearly affected by non-global contributions, since emissions outside of the jet can radiate energy into the jet. Because the soft drop procedure removes soft wide-angle radiation, we expect that the groomed jet energy E_g should have no non-global contributions. In principle, we could calculate the E_g distribution directly to show the absence of non-global logarithms. In practice, though, it is hard to interpret the meaning of E_g without invoking some reference energy scale. Here, we are using E_0 as a reference, which is not ideal since E_0 has non-global contributions. That said, we will find that the E_0 and Δ_E distributions have exactly the same non-global logarithms, implying that the E_g distribution is wholly absent of them.

Analogous to Sec. 3.4, we can do a simple calculation of the non-global contribution to Δ_E. At lowest order for a narrow jet of radius R_0, the non-global logarithms can be computed from

$$\frac{1}{\sigma_0} \frac{d\sigma^{\text{NG}}}{d\Delta_E} = 4 C_F C_A \left(\frac{\alpha_s}{2\pi}\right)^2 \int \frac{dz_1}{z_1} \frac{dz_2}{z_2} \int d\theta_1 \, d\theta_2 \frac{4\theta_1\theta_2}{\theta_1^2 \left(\theta_1^2 - \theta_2^2\right)} \Theta_{\text{NG}} \Theta \left(z_{\text{cut}} \frac{\theta_2^\beta}{R_0^\beta} - z_2\right) \delta(\Delta_E - z_2)$$

$$= \frac{2}{3} \pi^2 C_F C_A \left(\frac{\alpha_s}{2\pi}\right)^2 \frac{\log \frac{1}{\Delta_E}}{\Delta_E} + \mathcal{O}\left(R_0^2, \frac{\Delta_E^{2/\beta}}{z_{\text{cut}}^{2/\beta}}\right) \ . \tag{5.10}$$

This shows that non-global logarithms are not power-suppressed for the energy loss distribution regardless of β. Moreover, the coefficient of the non-global logarithms are the same for the ungroomed distribution ($\beta \to \infty$) as for the groomed distribution (finite β). This implies that the groomed jet energy E_g cannot contain any non-global logarithms.
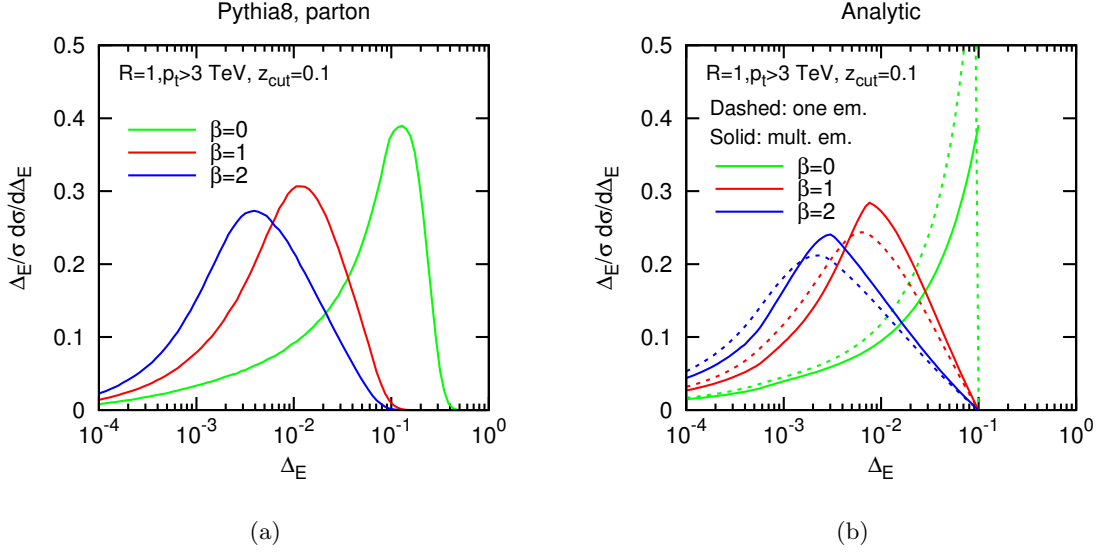
Figure 8: The distribution of groomed energy loss Δ_E in PYTHIA 8 (left) compared to our MLL calculation (right). In the MLL result, solid (dashed) corresponds to the distribution with (without) multiple emissions. The original jet radius is set to $R_0 = 1.0$ and the jets have an ungroomed energy of 3 TeV. The soft drop parameter $z_{\text{cut}} = 0.1$ is fixed while β is varied.

Of course, to really verify this behavior, one would want to calculate the groomed jet energy distribution in a process with an additional scale. For example, one could study the associated production of a photon and a jet (i.e. $pp \to \gamma + j$) and use the photon momentum as a reference scale. In this example, we would expect $(p_{Tg} - p_{T\gamma})/p_{T\gamma}$ should be free of non-global logarithms.

5.4   Comparison to Monte Carlo

We conclude this section by comparing the fractional energy loss distribution between PYTHIA 8 to our MLL calculation, using the same jet samples as Sec. 3.5. The comparison is shown in Fig. 8, with the Monte Carlo simulation on the left plot and our analytic calculation on the right. On the analytic plots, the solid (dashed) curves represent the result with (without) the inclusion of the multiple emission contributions to Δ_E.

For $\beta > 0$, there is good agreement between PYTHIA and our MLL analytics. For the IRC unsafe (but Sudakov safe) limit $\beta = 0$, the agreement is fair in the region $\Delta_E < z_{\text{cut}}$. Note that $\beta = 0$ has a large contribution from multiple emissions, but the structure of the inverse Laplace transform enforces that the MLL result cannot extend beyond $\Delta_E = z_{\text{cut}}$. In contrast, the PYTHIA distribution extends well beyond z_{cut}. This effect from multiple hard emissions contributing to $\Delta_E > z_{\text{cut}}$ is not captured by our resummation.
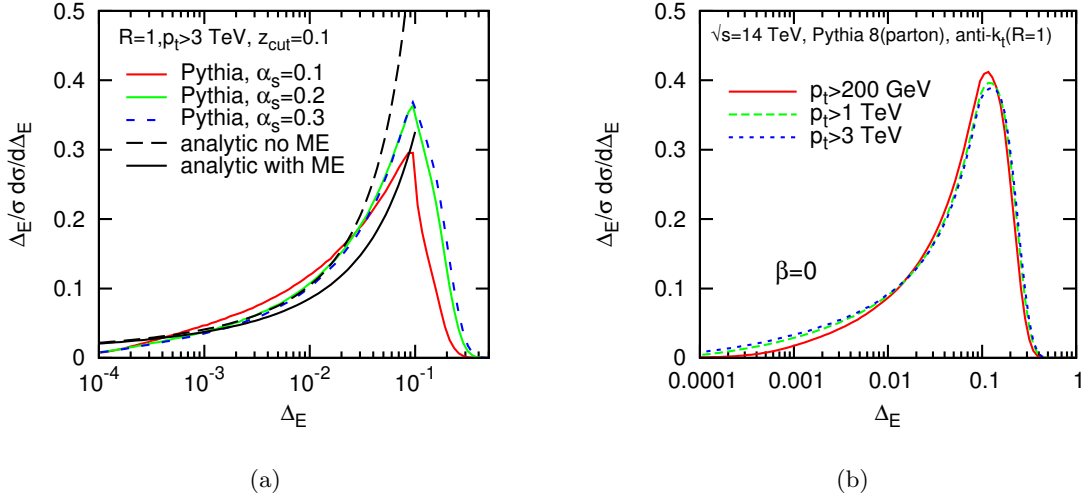
Figure 9: The dependence of the $\beta = 0$ energy drop distribution on α_s. On the left, we show PYTHIA results with fixed coupling compared to the fixed-coupling analytical prediction of Eq. (5.9). On the right, we show the Δ_E distribution with running coupling at different values of the jet's transverse momentum. Both plots support the interpretation that the Δ_E distribution at $\beta = 0$ is largely independent of α_s.

We can study the $\beta = 0$ limit in PYTHIA to see whether the analytic predictions of Sec. 5.2 are born out in Monte Carlo. In Fig. 9a, we show the Δ_E distribution for $\beta = 0$ by artificially turning off the running coupling and setting the α_s value by hand. As discussed in Eq. (5.9), the fixed-coupling analytic resummation does not depend on α_s. Indeed, we see that the Monte Carlo results are fairly independent of the α_s value, and the behavior is well described by the analytic calculation. The same physical effect is seen in Fig. 9b, where the running coupling is restored but the distribution is shown for different choices of the minimum transverse momentum of the jet, which in turn probes different values of α_s. We note that the curves differ very little from each other, suggesting that leading α_s-independence of the $\beta = 0$ result is robust.

6   Non-Perturbative Contributions

In all of the above analytic calculations, we only considered the distributions generated by perturbative partons. In this section, we will do a brief Monte Carlo study to try to estimate the impact that non-perturbative effects from hadronization and UE can have on these distributions.

In Fig. 10, we show the effect of hadronization (left) and UE (right) for various observables considered in this paper. In the case of hadronization, we plot the ratio between the hadronic and partonic distributions obtained from PYTHIA 8. In the case of UE, we plot the
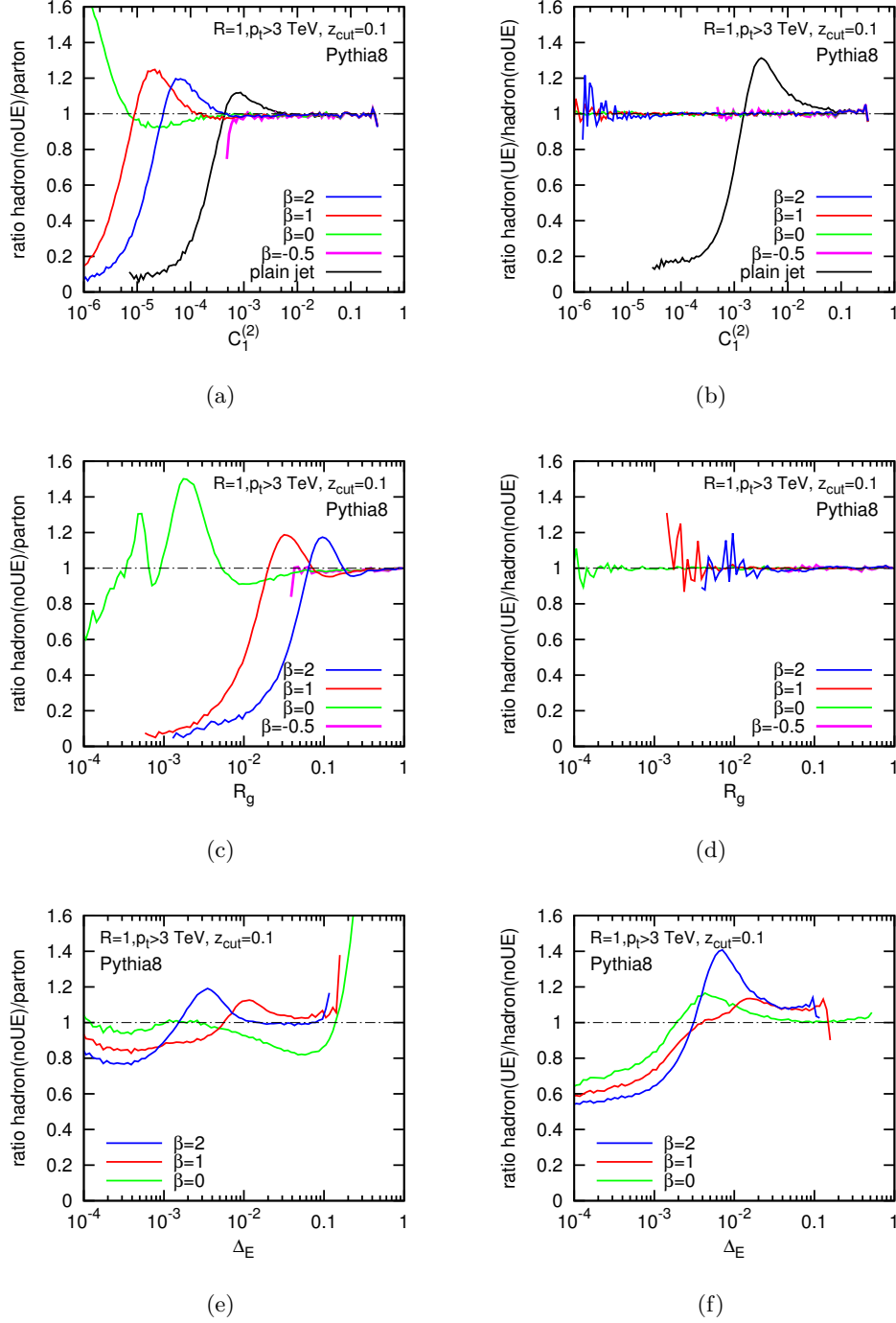
Figure 10: Effect of non-perturbative corrections on $C_1^{(\alpha=2)}$ (top), R_g (middle), and Δ_E (bottom). The plots on the left show the ratio between hadron level and parton level predictions obtained with PYTHIA 8 (without UE). The plots on the right instead show the ratio of hadron-level results with and without UE.

ratio between the distributions with and without UE. Apart from including non-perturbative effects, the details of the analysis are the same as for the previous Monte Carlo studies.

We start by considering $C_1^{(\alpha)}$ for $\alpha = 2$, i.e. similar to jet mass. The plot in Fig. 10a shows that soft drop declustering pushes the onset of hadronization corrections to smaller values of the observable compared to the ungroomed case (shown in black). As shown in Fig. 10b, soft drop has the remarkable ability to reduce the UE contribution to almost zero.

For the groomed jet radius distribution, the behavior of hadronization corrections in Fig. 10c is qualitatively similar to those seen for $C_1^{(\alpha)}$, with hadronization having a smaller effect for smaller values (and negative values) of β. The UE event contribution to R_g in Fig. 10d is also fairly small.

Finally, we show the effect of hadronization and UE corrections on the jet energy drop in Figs. 10e and 10f, respectively. Unlike for the previous distributions, the hadronization corrections are largest for $\beta = 0$, which is likely related to the issue of IRC unsafety. For all values of β, the UE corrections are fairly large for Δ_E. That said, because Δ_E is defined in terms of both the groomed energy E_g and the ungroomed energy E_0, it is hard to know whether these effects are caused mainly by E_g or E_0. We suspect that E_g is rather robust to UE effects, and the dominant change is really from distortions of the reference E_0 value.

7 Boosted W Tagging with Soft Drop

Thus far, we have studied the analytic properties of soft drop declustering and argued that it can be a successful grooming technique for $\beta > 0$. For $\beta < 0$, soft drop acts like a tagger which identifies jets with hard two-prong structures. Here, we investigate the performance of soft drop in tagging mode by doing a brief study of boosted W tagging.

To have a source of fat W and QCD jets, we generated WW and dijet samples with PYTHIA 8 for 14 TeV proton-proton collisions, including all non-perturbative effects from tune 4C. As in the previous Monte Carlo studies in this paper, we start from anti-k_t jets with $R_0 = 1$, this time keeping only jets with $p_T \geq p_{T\,\mathrm{min}}$ and rapidity $|y| < 4$. These samples of W (signal) and QCD (background) jets are then groomed/tagged using soft drop with various values of β and z_{cut}, and we define the efficiency/mistag rates from the fraction of selected jets after soft drop with groomed masses in the W window [70 GeV, 90 GeV].

The results of this study are presented in Figs. 11 and 12. In Fig. 11a, we fix $p_{T\,\mathrm{min}} = 500$ GeV and study the efficiency/mistag rates for fixed β, sweeping z_{cut}. The values of z_{cut} found as a function of the efficiency are shown in Fig. 11b. As initially expected, negative values of β (i.e. tagging mode) tend to have a higher performance than positive values (i.e. grooming mode). Note also that the z_{cut} values for $\beta < 0$ fall in the more reasonable range of $z_{\mathrm{cut}} \lesssim 1$, whereas $z_{\mathrm{cut}} \gtrsim 1$ is needed to obtain comparable performance for $\beta > 0$.

In Figs. 11c and 11d, we show the mass distributions of signal and background jets with $p_T > 500$ GeV after soft-drop, for different values of β and choosing the value of z_{cut} that correspond to 35% signal efficiency. Regarding the signal, all values of β yield a nice narrow mass distributions around m_W. Without soft drop, the background in this p_T window happens
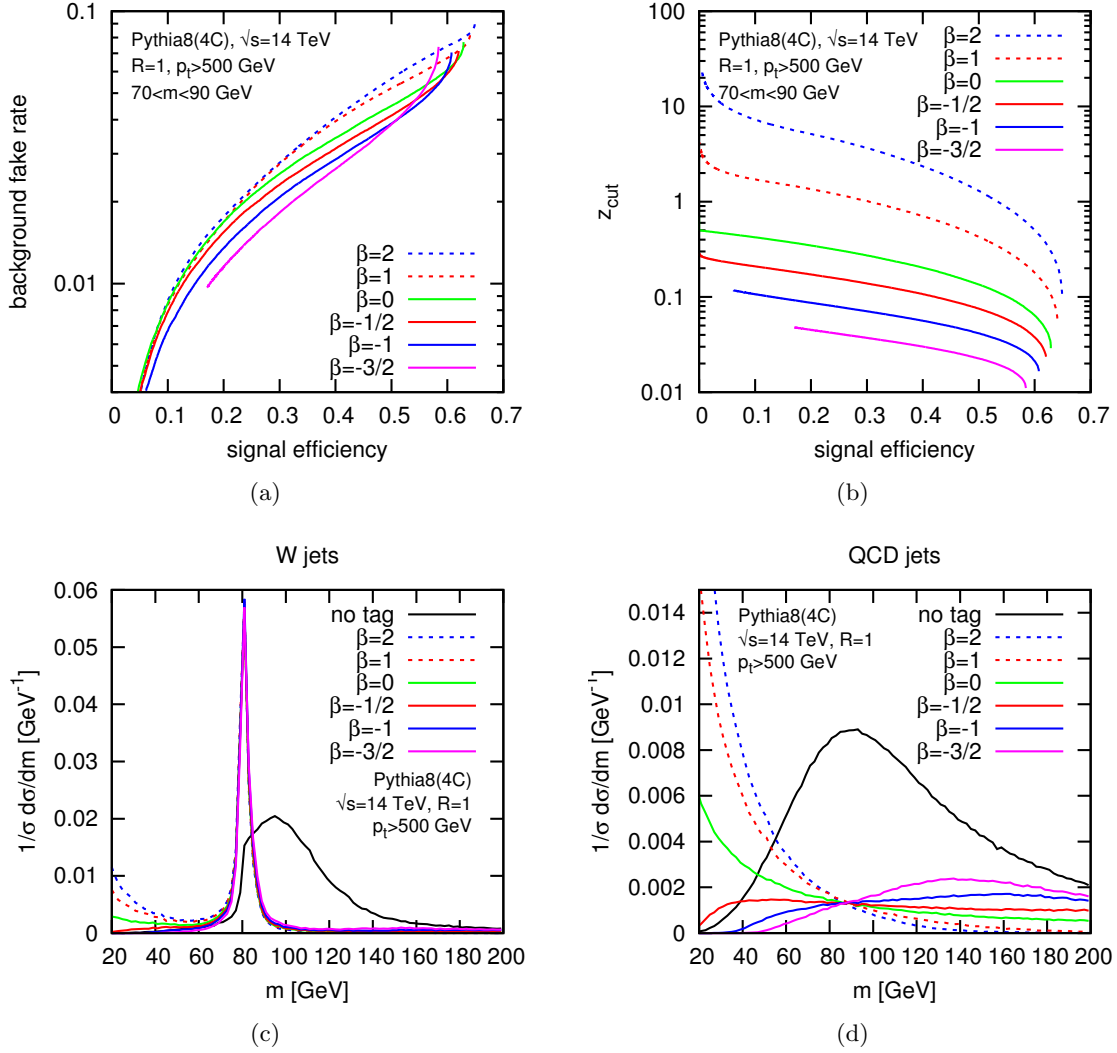
Figure 11: Performance of soft drop as a boosted W tagger. Top left: signal efficiency versus background mistag for jets with $p_T > 500$ GeV. Each curve is obtained by fixing the value of β, sweeping the value of z_{cut}, and counting jets with groomed mass in the range [70 GeV, 90 GeV]. Top right: Values of z_{cut} for as a function of the efficiency, for given β. Bottom: mass distribution of signal (left) and background (right) jets before and after soft drop. For each curve, the value of β is shown in the legend, while the value of z_{cut} is the one that gives a 35% signal efficiency.
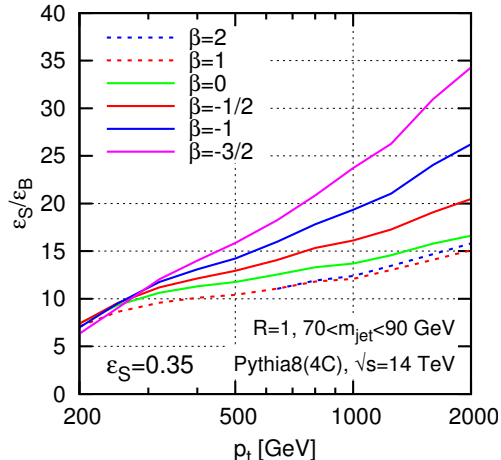
Figure 12: Ratio of signal-to-background efficiency as a function of the minimum jet p_T for fixed signal efficiency of 35%.

to (accidentally) have a mass peak around m_W, but as desired, the soft-dropped background mass distributions are pushed away from the signal region.

Finally, in Fig. 12, we study the ratio of signal-to-background efficiency as a function of $p_{T\,\mathrm{min}}$ (at fixed 35% signal efficiency). Negative values of β continue to have a higher performance, especially at large p_T, essentially because of a stronger Sudakov suppression of the background at fixed signal efficiency. The overall performance is comparable to other W tagging methods, with percent-level mistag rates at 35% efficiency.

The original mass-drop prescription from Ref. [6] also involves a filtering step. There, the filtering radius was taken as $\min(R_g/2, 0.3)$ with R_g defined as in Sec. 4, and the three hardest subjets were kept. However, applying filtering on soft-dropped jets is not necessarily beneficial. For example, at large p_T and for $\beta < 0$, the action of the soft drop is such that the background peaks at a value of the mass larger than the W mass. In this case, filtering would slightly shift this peak to smaller masses, increasing the background rates. On the other hand, we should add that in a situation with pileup, filtering or some similar form of grooming might also be needed in order to improve the resolution on the signal peak. We leave a detailed study of the interplay between pileup mitigation and boosted object tagging to future work.

8   Conclusions

In this paper, we introduced the soft drop declustering procedure. Soft drop generalizes the mMDT procedure by incorporating an angular exponent β, and simplifies mMDT by removing the mass drop condition. True to its name, the soft drop procedure drops wide-angle soft radiation from a jet, though for $\beta \leq 0$ it can also drop collinear radiation. To

demonstrate the analytic behavior of soft drop declustering, we calculated three distributions to MLL accuracy (while also including multiple emissions): the energy correlation functions $C_1^{(\alpha)}$, the groomed jet radius R_g, and the jet energy drop Δ_E. Two particularly interesting analytic features are the smooth turn off of non-global logarithms for $C_1^{(\alpha)}$ in the $\beta \to 0$ limit and the approximate α_s-independence of the jet energy drop distribution for $\beta = 0$.

Beyond our analytic calculations, we studied the performance of soft drop in two other contexts. We used a Monte Carlo study to estimate the impact of non-perturbative effects, and found that soft drop reduces the impact of hadronization and UE corrections on $C_1^{(\alpha)}$ compared to ungroomed case. We also used a Monte Carlo study to demonstrate that soft drop with $\beta < 0$ can act as an effective tagger for boosted W bosons.

One area for future study is the behavior of soft drop as a pileup mitigation tool. We have seen that soft drop yields small values of R_g and hence small jet areas, so one might expect that soft drop would have similar pileup performance to trimming [53, 69, 76, 89]. Like trimming, soft drop declustering with $\beta > 0$ is an all-purpose grooming procedure, in the sense that the grooming procedure does not veto jets (unlike a tagger), and the groomed version of an (otherwise) IRC safe observable is still IRC safe.[10] Both trimming and soft drop have two parameters. In the case of trimming, they are the energy fraction threshold f_{cut} and the subjet radius R_{sub}. In the case of soft drop, they are the soft drop threshold z_{cut} and the angular exponent β. The f_{cut} and z_{cut} parameters play a similar role, since they control how aggressive the grooming procedure is and also define the transition points in, e.g., the $C_1^{(\alpha)}$ distribution.

However, there is a qualitative difference between R_{sub} and β which is likely to be phenomenologically relevant. At fixed values of the jet mass, harder jets become narrower jets. The radius parameter R_{sub} sets a fixed angular scale, such that narrower jets are effectively groomed less (see the discussion in Ref. [59]). In contrast, β sets a scaling relation between energies and angles, such that the amount of grooming decreases only gradually as the jets become more narrow. The extreme limit of $\beta = 0$ is where approximately the same fraction of energy is groomed away regardless of the initial jet energy (see Eq. (5.9)). Thus, we expect that soft drop could potentially have better performance than trimming at higher energies and luminosities. Of course, this assumes that detectors are able to resolve angular scales smaller than the typical $R_{\text{sub}} \simeq 0.2$.

Finally, in a more speculative vein, one might wonder whether the soft drop procedure could be applied on an event-wide basis instead of jet-by-jet as considered here. In the case of trimming, there is a suitable generalization [127] such that the trimming criteria can be imposed without needing to first cluster an event into jets. In the case of mass drop, there are ways to sew together different jet multiplicities to impose a kind of event-wide mass drop condition [43]. If the soft drop condition in Eq. (1.1) could be applied on an event-wide basis,

---

[10]This is in contrast to the $\beta = 0$ (mMDT) limit, which has to be run in tagging mode to obtain an IRC safe groomed jet energy distribution. Of course, we have argued that $\beta = 0$ soft-dropped distributions are still Sudakov safe.

this could help address many of the numerous complications associated with soft radiation and allow analyses to focus on the more tractable collinear physics of jets.

Acknowledgments

A Details of Energy Correlation Calculation

We present the details of the calculation of the soft-drop energy correlation function ($C_1^{(\alpha)}$ with $\alpha > 0$) to MLL accuracy. Thus, we consider the independent emission of n collinear gluons within a jet. For each splitting m, the scale of the (one-loop) coupling is chosen at the relative transverse momentum scale $\kappa_m = z_m \theta_m p_{T\mathrm{jet}}$. This is sufficient to capture logarithmic accuracy we seek in this study (for a more detailed discussion, see the extensive literature on event-shape and jet-mass resummation, e.g. [114–116]).

The above undestanding translates into

$$
\begin{aligned}
\Sigma(C_1^{(\alpha)}) &= \sum_{n=0}^{\infty} \frac{1}{n!} \prod_{m=1}^{n} \int \frac{d\theta_m}{\theta_m} \int dz_m\, p_i(z_m) \frac{\alpha_s(\kappa_m)}{\pi} \left[\Theta\left(z_{\mathrm{cut}} \left(\frac{\theta_m}{R_0}\right)^{\beta} - z_m \right) \right. \\
&\quad + \left. \Theta\left(z_m - z_{\mathrm{cut}} \left(\frac{\theta_m}{R_0}\right)^{\beta} \right) \Theta\left(C_1^{(\alpha)} - z_m \left(\frac{\theta_m}{R_0}\right)^{\alpha} \right) - 1 \right] \Theta\left(R_0 - \theta_m \right) \\
&= \sum_{n=0}^{\infty} \frac{(-1)^n}{n!} \prod_{m=1}^{n} \int \frac{d\theta_m}{\theta_m} \int dz_m\, p_i(z_m) \frac{\alpha_s(\kappa_m)}{\pi} \left[\Theta\left(z_m \left(\frac{\theta_m}{R_0}\right)^{\alpha} - C_1^{(\alpha)} \right) \right. \\
&\quad \times \left. \Theta\left(z_m - z_{\mathrm{cut}} \left(\frac{\theta_m}{R_0}\right)^{\beta} \right) \right] \Theta\left(R_0 - \theta_m \right).
\end{aligned}
\tag{A.1}
$$

To MLL accuracy, the resummed result is then

$$
\Sigma(C_1^{(\alpha)}) = e^{-R(C_1^{(\alpha)})} \, ,
\tag{A.2}
$$

where the radiator is given by the integral of the one-loop contribution over the allowed phase-space:

$$
R(C_1^{(\alpha)}) = \frac{1}{\alpha} \int_{C_1^{(\alpha)}}^{1} \frac{dc}{c} \int_{\max\left(c,\, z_{\mathrm{cut}}^{\frac{\alpha}{\alpha+\beta}} c^{\frac{\beta}{\alpha+\beta}} \right)}^{1} dz\, p_i(z) \frac{\alpha_s(\kappa)}{\pi} \, .
\tag{A.3}
$$

The reduced splitting functions p_i, with $i = q, g$ are given by

$$p_q(z) = C_F \frac{1 + (1-z)^2}{z} \,, \tag{A.4a}$$

$$p_g(z) = C_A \left[2\frac{1-z}{z} + z(1-z) + \frac{T_R n_f}{C_A}(z^2 + (1-z)^2) \right] . \tag{A.4b}$$

Note that for small enough values of energy fractions z and angular distances θ, the argument of the coupling in Eq. (A.3) can approach the non-perturbative region. Thus, we introduce a prescription in order to evaluate the integrals down to these low scales. We decide to freeze the coupling below a non-perturbative scale μ_{NP}:

$$\alpha_s(\kappa) = \alpha_s^{\text{1-loop}}(\kappa)\Theta\left(\kappa - \mu_{\mathrm{NP}}\right) + \alpha_s^{\text{1-loop}}(\mu_{\mathrm{NP}})\Theta\left(\mu_{\mathrm{NP}} - \kappa\right) , \tag{A.5}$$

where $\alpha_s^{\text{1-loop}}(\kappa)$ is the usual one-loop expression for the strong coupling, i.e. its running is evaluated with β_0 only:

$$\alpha_s^{\text{1-loop}}(\kappa) = \frac{\alpha_s(Q)}{1 + 2\alpha_s(Q)\beta_0 \log \frac{\kappa}{Q}} \,. \tag{A.6}$$

Our results are expressed in terms of $\alpha_s = \alpha_s(R_0\, p_T)$ and we use $\alpha_s(m_Z) = 0.12$, $n_f = 5$, and $\mu_{\mathrm{NP}} = 1$ GeV throughout this paper.

In the $(\log \frac{1}{z}, \log \frac{R_0}{\theta})$ plane of Fig. 2, the boundary between perturbative and non-perturbative regions is given by

$$\kappa = \mu_{\mathrm{NP}} \quad \Rightarrow \quad \log \frac{1}{z} = \log \frac{1}{\tilde{\mu}} - \log \frac{R_0}{\theta}, \tag{A.7}$$

where we have introduced $\tilde{\mu} = \frac{\mu_{\mathrm{NP}}}{p_T R_0}$. Thus, according to Eq. (A.5), below this straight line, the one-loop running coupling is evaluated at the relative transverse momentum κ, while above this line it is frozen at μ_{NP}.

The explicit form for the non-perturbative region of result depends on the relation between the slope of lines of constant $C_1^{(\alpha)}$, which is controlled by α, and the slope of the boundary between perturbative and non-perturbative regime, given by Eq. (A.7). We also assume $\beta \geq 0$ for simplicity and discuss the case $\beta < 0$ in the end.

For $\alpha > 1$ we find

$$R(C_1^{(\alpha)}) \overset{C_1^{(\alpha)} \geq z_{\mathrm{cut}}}{=} \frac{C_i}{2\pi\alpha_s\beta_0^2} \left[\frac{\mathrm{W}(1-\lambda)}{\alpha - 1} - \frac{\alpha\mathrm{W}(1-\frac{1}{\alpha}\lambda)}{\alpha - 1} - 2\alpha_s\beta_0 B_i \log(1 - \frac{1}{\alpha}\lambda) \right] \tag{A.8}$$

$$\overset{z_{\mathrm{cut}}^{\frac{1-\alpha}{1+\beta}}\tilde{\mu}^{\frac{\alpha+\beta}{1+\beta}} \leq C_1^{(\alpha)} < z_{\mathrm{cut}}}{=} \frac{C_i}{2\pi\alpha_s\beta_0^2} \Bigg[-\frac{\mathrm{W}(1-\lambda_c)}{1+\beta} - \frac{\alpha\mathrm{W}(1-\frac{1}{\alpha}\lambda)}{\alpha - 1} - 2\alpha_s\beta_0 B_i \log(1 - \frac{1}{\alpha}\lambda)$$

$$+ \frac{\alpha+\beta}{(\alpha-1)(1+\beta)}\mathrm{W}\left(1 - \frac{1+\beta}{\alpha+\beta}\lambda - \frac{\alpha-1}{\alpha+\beta}\lambda_c\right) \Bigg] \tag{A.9}$$

$$\overset{\tilde{\mu}^{\alpha} < C_1^{(\alpha)} \leq z_{\mathrm{cut}}^{\frac{1-\alpha}{1+\beta}}\tilde{\mu}^{\frac{\alpha+\beta}{1+\beta}}}{=} \frac{C_i}{2\pi\alpha_s\beta_0^2} \Bigg[-\frac{\mathrm{W}(1-\lambda_c)}{1+\beta} - \frac{\alpha\mathrm{W}(1-\frac{1}{\alpha}\lambda)}{\alpha - 1} - 2\alpha_s\beta_0 B_i \log(1 - \frac{1}{\alpha}\lambda)$$

$$- \frac{1 + \log\left(1 - \lambda_\mu\right)}{(\alpha-1)(1+\beta)} \left((\alpha - 1)\lambda_c + (1+\beta)\lambda - (\alpha+\beta)\lambda_\mu\right)$$

$$+ \frac{\alpha + \beta}{(\alpha - 1)(1 + \beta)} W\left(1 - \lambda_\mu\right)\bigg] + \frac{C_i \alpha_s(\mu_{\mathrm{NP}})}{\pi} \mathcal{F}_1(L) \qquad (\mathrm{A.10})$$

$$\stackrel{C_1^{(\alpha)} < \tilde{\mu}^\alpha}{=} \frac{C_i}{2\pi\alpha_s\beta_0^2}\bigg[-\frac{\mathrm{W}(1 - \lambda_c)}{1 + \beta} - \frac{\beta \mathrm{W}(1 - \lambda_\mu)}{1 + \beta} - 2\alpha_s\beta_0 B_i \log(1 - \lambda_\mu)$$

$$-\frac{1 + \log\left(1 - \lambda_\mu\right)}{(1 + \beta)}\left(\lambda_c + \beta\lambda_\mu\right)\bigg] + \frac{C_i \alpha_s(\mu_{\mathrm{NP}})}{\pi}\bigg[\mathcal{F}_1(\alpha\, L_\mu)$$

$$+\left(\frac{L}{\alpha} - L_\mu\right)\left(\frac{2\alpha}{\alpha + \beta}L_c + 2B_i + \frac{\beta}{\alpha + \beta}(L + \alpha L_\mu)\right)\bigg], \qquad (\mathrm{A.11})$$

while for $\alpha < 1$ we have[11]

$$R(C_1^{(\alpha)}) \stackrel{C_1^{(\alpha)} \geq z_{\mathrm{cut}}}{=} \frac{C_i}{2\pi\alpha_s\beta_0^2}\bigg[\frac{\mathrm{W}(1 - \lambda)}{\alpha - 1} - \frac{\alpha \mathrm{W}(1 - \frac{1}{\alpha}\lambda)}{\alpha - 1} - 2\alpha_s\beta_0 B_i \log(1 - \frac{1}{\alpha}\lambda)\bigg] \qquad (\mathrm{A.12})$$

$$\stackrel{\tilde{\mu}^\alpha < C_1^{(\alpha)} < z_{\mathrm{cut}}}{=} \frac{C_i}{2\pi\alpha_s\beta_0^2}\bigg[-\frac{\mathrm{W}(1 - \lambda_c)}{1 + \beta} - \frac{\alpha \mathrm{W}(1 - \frac{1}{\alpha}\lambda)}{\alpha - 1} - 2\alpha_s\beta_0 B_i \log(1 - \frac{1}{\alpha}\lambda)$$

$$+ \frac{\alpha + \beta}{(\alpha - 1)(1 + \beta)}\mathrm{W}\left(1 - \frac{1 + \beta}{\alpha + \beta}\lambda - \frac{\alpha - 1}{\alpha + \beta}\lambda_c\right)\bigg] \qquad (\mathrm{A.13})$$

$$\stackrel{z_{\mathrm{cut}}^{\frac{1-\alpha}{1+\beta}} \tilde{\mu}^{\frac{\alpha+\beta}{1+\beta}} < C_1^{(\alpha)} < \tilde{\mu}^\alpha}{=} \frac{C_i}{2\pi\alpha_s\beta_0^2}\bigg[-\frac{\mathrm{W}(1 - \lambda_c)}{1 + \beta} - \frac{\alpha \mathrm{W}(1 - \lambda_\mu)}{\alpha - 1} + \frac{\lambda - \alpha\lambda_\mu}{\alpha - 1}\left(1 + \log(1 - \lambda_\mu)\right)$$

$$- 2\alpha_s\beta_0 B_i \log(1 - \lambda_\mu) + \frac{\alpha + \beta}{(\alpha - 1)(1 + \beta)}\mathrm{W}\left(1 - \frac{1 + \beta}{\alpha + \beta}\lambda - \frac{\alpha - 1}{\alpha + \beta}\lambda_c\right)\bigg]$$

$$+ \frac{C_i \alpha_s(\mu_{\mathrm{NP}})}{\pi}\left(\frac{L}{\alpha} - L_\mu\right)\left(\frac{L - \alpha L_\mu}{1 - \alpha} + 2B_i\right) \qquad (\mathrm{A.14})$$

$$\stackrel{C_1^{(\alpha)} < z_{\mathrm{cut}}^{\frac{1-\alpha}{1+\beta}} \tilde{\mu}^{\frac{\alpha+\beta}{1+\beta}}}{=} \frac{C_i}{2\pi\alpha_s\beta_0^2}\bigg[-\frac{\mathrm{W}(1 - \lambda_c)}{1 + \beta} - \frac{\beta \mathrm{W}(1 - \lambda_\mu)}{1 + \beta} - \left(\frac{\lambda_c + \beta\lambda_\mu}{1 + \beta}\right)$$

$$\times \left(1 + \log(1 - \lambda_\mu)\right) - 2\alpha_s\beta_0 B_i \log(1 - \lambda_\mu)\bigg]$$

$$+ \frac{C_i \alpha_s(\mu_{\mathrm{NP}})}{\pi}\bigg[\mathcal{F}_2(L) + \frac{(1 - \alpha)(\beta L_\mu + L_c)(2(1 + \beta)B_i + \beta L_\mu + L_c)}{\alpha(1 + \beta)^2}\bigg]. \qquad (\mathrm{A.15})$$

In the above expressions, we have introduced $\mathrm{W}(x) = x \log x$ and

$$\mathcal{F}_1(L) = \frac{((1 + \beta)L - (\alpha + \beta)L_\mu + (\alpha - 1)L_c)^2}{(\alpha - 1)(1 + \beta)(\alpha + \beta)}, \qquad (\mathrm{A.16})$$

$$\mathcal{F}_2(L) = \frac{(1 + \beta)L - (\alpha + \beta)L_\mu + (\alpha - 1)L_c}{\alpha(1 + \beta)^2(\alpha + \beta)} \qquad (\mathrm{A.17})$$

$$\times \left(\beta\left(\alpha + \beta\right)L_\mu + 2B_i(1 + \beta)(\alpha + \beta) + L_c(2\alpha + \alpha\beta + \beta) + \beta\left(1 + \beta\right)L\right).$$

Here, C_i is the color of the jet appropriate for quarks ($C_q = C_F$) or gluons ($C_g = C_A$). B_i describes the contribution to the cross section from collinear logarithms: $B_q = -3/4$ for quark

---

[11]For definiteness we consider the case $z_{\mathrm{cut}} > \tilde{\mu}^\alpha$.

jets and $B_g = -\frac{11}{12} + \frac{n_f}{6C_A}$ for gluon jets, where n_f is the number of active quark flavors. We have also introduced

$$L = \log(1/C_1^{(\alpha)}) \qquad\qquad L_c = \log(1/z_{\rm cut}) \qquad\qquad L_\mu = \log(1/\tilde{\mu}), \qquad\qquad \text{(A.18)}$$

$$\lambda = 2\alpha_s \beta_0 L \qquad\qquad \lambda_c = 2\alpha_s \beta_0 L_c \qquad\qquad \lambda_\mu = 2\alpha_s \beta_0 L_\mu. \qquad\qquad \text{(A.19)}$$

Moreover, it can be easily checked that the limit $\alpha \to 1$ is perfectly safe because the two non-perturbative transition points coincide and therefore one non-perturbative region disappears.

We note that expression for the running coupling with non-perturbative freezing Eq. (A.5) has a discontinuous first derivative at $\kappa = \mu_{\rm NP}$. To our logarithmic accuracy, this behavior is reflected into a discontinuity of the second derivative of the radiator at $C_1^{(\alpha)} = \tilde{\mu}^\alpha$, which in turns causes a kink in the spectrum. The difference between right- and left- second derivatives of the radiator at $C_1^{(\alpha)} = \tilde{\mu}^\alpha$ is

$$c = \left(\frac{\alpha_s(\mu_{\rm NP})}{\pi}\right)^2 \frac{4\pi \beta_0 C_F B_i}{\alpha^2}, \qquad\qquad \text{(A.20)}$$

which is a contribution beyond the accuracy of our calculation. This effect is bigger for smaller α, and for the case $\alpha = 0.5$ in Fig. 4f, the non-perturbative transition point $C_1^{(\alpha)} = \tilde{\mu}^\alpha$ occurs in the vicinity of the Sudakov peak. Clearly, this is an artefact of our choice of an abrupt freezing of the coupling in the non-perturbative region. One could imagine to alter Eq. (A.5) in such a way that it smoothly interpolates between running and fixed coupling (as done, for example, with scale profiling [128]). Alternatively, one could add an appropriate (subleading) term to the radiator in the region $C_1^{(\alpha)} < \tilde{\mu}^\alpha$. However, we have decided not to introduce an ad-hoc prescription and, in this paper, we present results obtained from our MLL calculations (plus eventually multiple-emission effects), with the freezing of coupling previously discussed.

As already mentioned, the results for the resummed exponent have been obtained assuming $\beta > 0$. It is clear from the expressions above that the $\beta \to 0$ limit is perfectly safe. Indeed for $\beta = 0$ the result considerably simplifies and one obtains the mMDT single-logarithmic distribution. Moreover, the same results also hold for the $\beta < 0$ case, provided that $C_1^{(\alpha)} > z_{\rm cut}^{\alpha/|\beta|}$, which is the minimum allowed value for the energy correlation function. For $C_1^{(\alpha)} < z_{\rm cut}^{\alpha\|\beta\|}$, the radiator freezes at $R\left(z_{\rm cut}^{\alpha/|\beta|}\right)$ and consequently the differential distribution vanishes.

Finally, the above results are also sufficient to compute the multiple-emission contributions described in Sec. 3.3, which simply involve the derivative, as defined in Eq. (3.16), of the radiator functions derived in this appendix.

B   Details of Jet Radius Calculation

Here, we present the details of the calculation of the cumulative cross section of the jet radius after soft drop declustering. Because we are interested in the behavior of soft drop as a grooming procedure, we only consider $\beta > 0$. As presented in Sec. 4, the cumulative

resummed cross section can be computed from the sum over emissions as

$$\Sigma^{\text{radius}}(R_g) = \sum_{n=1}^{\infty} \frac{1}{n!} \prod_{m=1}^{n} \left[\int_{R_g}^{R_0} \frac{d\theta_m}{\theta_m} \int_0^1 dz_m \, p_i(z_m) \frac{\alpha_s(\kappa_m)}{\pi} \Theta \left(z_{\text{cut}} \frac{\theta_m^\beta}{R_0^\beta} - z_m \right) \right]$$
$$\times \, e^{-\int_{R_g}^{R_0} \frac{d\theta}{\theta} \int_0^1 dz \, p_i(z) \frac{\alpha_s(\kappa)}{\pi}}$$
$$= e^{-R_1(R_g)} \,, \tag{B.1}$$

where the exponent $R_1(R_g)$ is given by

$$R_1(R_g) = \int_{R_g}^{R_0} \frac{d\theta}{\theta} \int_0^1 dz \, p_i(z) \frac{\alpha_s(\kappa)}{\pi} \Theta \left(z - z_{\text{cut}} \frac{\theta^\beta}{R_0^\beta} \right) \,. \tag{B.2}$$

The evaluation of the integrals proceed analogously to the case of the energy correlation case described in detail in App. A. In this case, the radiator is found to be

$$R_1(R_g) \overset{R_g > R_g^{(0)}}{=} \frac{C_i}{2\pi\alpha_s\beta_0^2} \left[-W(1-\lambda_g) - \frac{W(1-\lambda_c)}{1+\beta} + \frac{1}{1+\beta}W(1-\lambda_c - (1+\beta)\lambda_g) \right.$$
$$\left. - 2\alpha_s\beta_0 B_i \log(1-\lambda_g) \right] \tag{B.3}$$

$$\overset{\mu R_0 < R_g < R_g^{(0)}}{=} \frac{C_i}{2\pi\alpha_s\beta_0^2} \left[-W(1-\lambda_g) - \frac{W(1-\lambda_c)}{1+\beta} + \frac{1-\lambda_c - (1+\beta)\lambda_g}{1+\beta} \log(1-\lambda_\mu) \right.$$
$$\left. + \frac{\lambda_\mu - \lambda_c - (1+\beta)\lambda_g}{1+\beta} - 2\alpha_s\beta_0 B_i \log(1-\lambda_g) \right]$$
$$+ \frac{C_i\alpha_s(\mu_{\text{NP}})}{\pi} \frac{1}{1+\beta} \left[(1+\beta)L_g + L_c - L_\mu \right]^2 \tag{B.4}$$

$$\overset{R_g \leq \mu R_0}{=} \frac{C_i}{2\pi\alpha_s\beta_0^2} \left[-\frac{W(1-\lambda_c)}{1+\beta} - \frac{\lambda_c+\beta}{1+\beta} \log(1-\lambda_\mu) - \frac{\lambda_c + \beta\lambda_\mu}{1+\beta} \right.$$
$$\left. - 2\alpha_s\beta_0 B_i \log(1-\lambda_\mu) \right]$$
$$+ \frac{C_i\alpha_s(\mu_{\text{NP}})}{\pi} \left[\frac{1}{1+\beta}(\beta L_\mu + L_c)^2 + (L_g - L_\mu)(\beta L_g + \beta L_\mu + 2L_c + 2B_i) \right] \tag{B.5}$$

with $R_g^{(0)} = R_0(\tilde{\mu}/z_{\text{cut}})^{1/(1+\beta)}$ and $L_g = \log(R_0/R_g)$, $\lambda_g = 2\alpha_s\beta_0 L_g$.

C   Details of Energy Drop Calculation

Here, we present the details of the calculation of the cumulative cross section for the fractional energy drop from soft drop declustering. Because we are interested in behavior of soft drop as a grooming procedure, we only consider $\beta > 0$. As opposed to the calculations previously described, for the energy drop distribution we also consider the effect of multiple emissions.

The resummed cumulative distribution is most easily written at fixed groomed jet radius R_g. The resulting expression is then integrated over all possible values of R_g:

$$\Sigma^{\text{energy-drop}}(\Delta_E) = \int_0^{R_0} dR_g \, \frac{d\Sigma^{\text{radius}}(R_g)}{dR_g} \int \frac{d\nu}{2\pi i \nu} e^{\nu \Delta_E} e^{-R_2(R_g, \nu^{-1})} \, , \qquad \text{(C.1)}$$

and $R_2(R_g, \nu)$ is the radiator function:

$$R_2(R_g, \nu^{-1}) = \int_{R_g}^{R_0} \frac{d\theta}{\theta} \int_0^1 dz \, p_i(z) \frac{\alpha_s(\kappa)}{\pi} \Theta\left(z_{\text{cut}} \frac{\theta^\beta}{R_0^\beta} - z\right) (1 - e^{-\nu z}) \, , \qquad \text{(C.2)}$$

In order to capture the single-logarithmic terms in Eq. (C.2) arising from multiple emissions we can make the following simplification [114–116]

$$R_2(R_g, \nu^{-1}) \simeq \bar{R}_2(R_g, \nu^{-1}) + \gamma_E \bar{R}_2'(R_g, \nu^{-1}) \, , \qquad \text{(C.3)}$$

where

$$\bar{R}_2(R_g, \nu^{-1}) = 2 \int_{R_g}^{R_0} \frac{d\theta}{\theta} \int_{\nu^{-1}}^1 \frac{dz}{z} \frac{\alpha_s(\kappa)}{\pi} \Theta\left(z_{\text{cut}} \frac{\theta^\beta}{R_0^\beta} - z\right) \, , \qquad \text{(C.4)}$$

γ_E is the Euler-Mascheroni constant and $\bar{R}_2'(R_g, \nu^{-1})$ is the logarithmic derivative of $\bar{R}_2$ with respect to ν. Moreover, note that we were able to drop the finite contributions to the splitting function $p_i(z)$ because for small values of z_{cut}, there are no logarithms from hard collinear emission.

The inverse Laplace transform in Eq. (C.1) can be done to single logarithmic accuracy in ν, also, by expanding ν about a fixed value ν_0. Doing this, the inverse Laplace transform becomes

$$\int \frac{d\nu}{2\pi i \nu} e^{\nu \Delta_E} e^{-R_2(R_g, \nu^{-1})} = \frac{(\nu_0 \Delta_E)^{-\bar{R}_2'(R_g, \nu_0^{-1})}}{\Gamma\left(1 + \bar{R}_2'(R_g, \nu_0^{-1})\right)} e^{-\bar{R}_2(R_g, \nu_0^{-1}) - \gamma_E \bar{R}_2'(R_g, \nu_0^{-1})} \, . \qquad \text{(C.5)}$$

To minimize the logarithms, we choose $\nu_0 = \Delta_E^{-1}$ and so the cumulative distribution of the groomed jet energy drop becomes

$$\Sigma^{\text{energy-drop}}(\Delta_E) = \int_0^{R_0} dR_g \, \frac{d\Sigma^{\text{radius}}(R_g)}{dR_g} \frac{e^{-\gamma_E \bar{R}_2'(R_g, \Delta_E)}}{\Gamma(1 + \bar{R}_2'(R_g, \Delta_E))} e^{-\bar{R}_2(R_g, \Delta_E)} \, , \qquad \text{(C.6)}$$

The evaluation of the integrals with running coupling proceeds in the same way as discussed for the energy correlation and groomed-jet radius distributions. We first obtain the energy drop cumulative distribution at fixed R_g and then numerically integrate of R_g. The radiator $\bar{R}_2$ is better described in three regions of R_g. First, for $R_g > R_0(\tilde{\mu}/z_{\text{cut}})^{1/(1+\beta)}$, we find

$$\bar{R}_2(\Delta_E) \overset{\Delta_E > z_{\text{cut}}(R_g/R_0)^\beta}{=} \frac{C_i}{2\pi \alpha_s \beta_0^2} \left[\frac{\text{W}(1 - \lambda_c)}{1 + \beta} - \text{W}(1 - \lambda_E) + \frac{\beta}{1 + \beta} \text{W}\left(1 + \frac{\lambda_c - (1+\beta)\lambda_E}{\beta}\right) \right]$$

$$\text{(C.7)}$$

$$\overset{\tilde{\mu}R_0/R_g < \Delta_E \leq z_{\rm cut}(R_g/R_0)^\beta}{=} \frac{C_i}{2\pi\alpha_s\beta_0^2}\left[\frac{{\rm W}(1-\lambda_c)}{1+\beta} - {\rm W}(1-\lambda_E) - \frac{{\rm W}(1-\lambda_c-(1+\beta)\lambda_g)}{1+\beta}\right.$$
$$\left. + {\rm W}(1-\lambda_g-\lambda_E)\right] \tag{C.8}$$

$$\overset{\tilde{\mu} < \Delta_E \leq \tilde{\mu}R_0/R_g}{=} \frac{C_i}{2\pi\alpha_s\beta_0^2}\left[\frac{{\rm W}(1-\lambda_c)}{1+\beta} - {\rm W}(1-\lambda_E) - \frac{{\rm W}(1-\lambda_c-(1+\beta)\lambda_g)}{1+\beta}\right.$$
$$\left. + (1-\lambda_g-\lambda_E)\log(1-\lambda_\mu) + (\lambda_\mu-\lambda_g-\lambda_E)\right]$$
$$+ \frac{C_i\alpha_s(\mu_{\rm NP})}{\pi}(L_g+L_E-L_\mu)^2 \tag{C.9}$$

$$\overset{\Delta_E < \tilde{\mu}}{=} \frac{C_i}{2\pi\alpha_s\beta_0^2}\left[\frac{{\rm W}(1-\lambda_c)}{1+\beta} - \frac{{\rm W}(1-\lambda_c-(1+\beta)\lambda_g)}{1+\beta} - \lambda_g\log(1-\lambda_\mu) - \lambda_g\right]$$
$$+ \frac{C_i\alpha_s(\mu_{\rm NP})}{\pi}L_g(L_g+2L_E-2L_\mu). \tag{C.10}$$

Then, for $(\tilde{\mu}/z_{\rm cut})^{1/\beta} < R_g/R_0 < (\tilde{\mu}/z_{\rm cut})^{1/(1+\beta)}$, we find

$$\bar{R}_2(\Delta_E) \overset{\Delta_E > \Delta_E^{(0)}}{=} \frac{C_i}{2\pi\alpha_s\beta_0^2}\left[\frac{{\rm W}(1-\lambda_c)}{1+\beta} - {\rm W}(1-\lambda_E) + \frac{\beta}{1+\beta}{\rm W}\left(1+\frac{\lambda_c-(1+\beta)\lambda_E}{\beta}\right)\right] \tag{C.11}$$

$$\overset{z_{\rm cut}(R_g/R_0)^\beta < \Delta_E < \Delta_E^{(0)}}{=} \frac{C_i}{2\pi\alpha_s\beta_0^2}\left[\frac{{\rm W}(1-\lambda_c)}{1+\beta} - {\rm W}(1-\lambda_E) + \frac{\beta+\lambda_c-(1+\beta)\lambda_E}{1+\beta}\log(1-\lambda_\mu)\right.$$
$$\left. + \frac{\lambda_c+\beta\lambda_\mu-(1+\beta)\lambda_E}{1+\beta}\right] + \frac{C_i\alpha_s(\mu_{\rm NP})}{\pi}\frac{1+\beta}{\beta}\left(L_E - \frac{L_c+\beta L_\mu}{1+\beta}\right)^2 \tag{C.12}$$

$$\overset{\tilde{\mu} < \Delta_E < z_{\rm cut}(R_g/R_0)^\beta}{=} \frac{C_i}{2\pi\alpha_s\beta_0^2}\left[\frac{{\rm W}(1-\lambda_c)}{1+\beta} - {\rm W}(1-\lambda_E) + \frac{\beta+\lambda_c-(1+\beta)\lambda_E}{1+\beta}\log(1-\lambda_\mu)\right.$$
$$\left. + \frac{\lambda_c+\beta\lambda_\mu-(1+\beta)\lambda_E}{1+\beta}\right]$$
$$+ \frac{C_i\alpha_s(\mu_{\rm NP})}{\pi}\left[(L_E+L_g-L_\mu)^2 - \frac{(L_c+(1+\beta)L_g-L_\mu)^2}{1+\beta}\right] \tag{C.13}$$

$$\overset{\Delta_E < \tilde{\mu}}{=} \frac{C_i}{2\pi\alpha_s\beta_0^2}\left[\frac{{\rm W}(1-\lambda_c)}{1+\beta} - \frac{1-\lambda_c}{1+\beta}\log(1-\lambda_\mu) + \frac{\lambda_c-\lambda_\mu}{1+\beta}\right.$$
$$+ \frac{C_i\alpha_s(\mu_{\rm NP})}{\pi}\left[L_g^2 - \frac{(L_c+(1+\beta)L_g-L_\mu)^2}{1+\beta} + 2L_g(L_E-L_\mu)\right], \tag{C.14}$$

with $\Delta_E^{(0)} = (z_{\rm cut}\tilde{\mu}^\beta)^{1/(1+\beta)}$. Finally, for $R_g/R_0 < (\tilde{\mu}/z_{\rm cut})^{1/\beta}$,

$$\bar{R}_2(\Delta_E) \overset{\Delta_E > \Delta_E^{(0)}}{=} \frac{C_i}{2\pi\alpha_s\beta_0^2}\left[\frac{{\rm W}(1-\lambda_c)}{1+\beta} - {\rm W}(1-\lambda_E) + \frac{\beta}{1+\beta}{\rm W}\left(1+\frac{\lambda_c-(1+\beta)\lambda_E}{\beta}\right)\right] \tag{C.15}$$

$$\overset{\tilde{\mu}<\Delta_E<\Delta_E^{(0)}}{=} \frac{C_i}{2\pi\alpha_s\beta_0^2}\left[\frac{\mathrm{W}(1-\lambda_c)}{1+\beta} - \mathrm{W}(1-\lambda_E) + \frac{\beta+\lambda_c-(1+\beta)\lambda_E}{1+\beta}\log(1-\lambda_\mu)\right.$$
$$\left. + \frac{\lambda_c+\beta\lambda_\mu-(1+\beta)\lambda_E}{1+\beta}\right] + \frac{C_i\alpha_s(\mu_{\mathrm{NP}})}{\pi}\frac{1+\beta}{\beta}\left(L_E - \frac{L_c+\beta L_\mu}{1+\beta}\right)^2$$

(C.16)

$$\overset{z_{\mathrm{cut}}(R_g/R_0)^\beta<\Delta_E<\tilde{\mu}}{=} \frac{C_i}{2\pi\alpha_s\beta_0^2}\left[\frac{\mathrm{W}(1-\lambda_c)}{1+\beta} - \frac{1-\lambda_c}{1+\beta}\log(1-\lambda_\mu) + \frac{\lambda_c-\lambda_\mu}{1+\beta}\right]$$
$$+ \frac{C_i\alpha_s(\mu_{\mathrm{NP}})}{\pi}\left[\frac{(L_E-L_c)^2}{\beta} - \frac{(L_\mu-L_c)^2}{1+\beta}\right]$$

(C.17)

$$\overset{\Delta_E<z_{\mathrm{cut}}(R_g/R_0)^\beta}{=} \frac{C_i}{2\pi\alpha_s\beta_0^2}\left[\frac{\mathrm{W}(1-\lambda_c)}{1+\beta} - \frac{1-\lambda_c}{1+\beta}\log(1-\lambda_\mu) + \frac{\lambda_c-\lambda_\mu}{1+\beta}\right]$$
$$+ \frac{C_i\alpha_s(\mu_{\mathrm{NP}})}{\pi}\left[\beta L_g^2 - \frac{(L_\mu-L_c)^2}{1+\beta} + 2L_g(L_E-L_c-\beta L_g)\right].$$

(C.18)

In the above expressions, we have introduced $L_E = \log(1/\Delta_E)$ and $\lambda_E = 2\alpha_s\beta_0 L_E$.

References

[1] A. Abdesselam, E. B. Kuutmann, U. Bitenc, G. Brooijmans, J. Butterworth, et al., *Boosted objects: A Probe of beyond the Standard Model physics*, *Eur.Phys.J.* **C71** (2011) 1661, [arXiv:1012.5412].

[2] A. Altheimer, S. Arora, L. Asquith, G. Brooijmans, J. Butterworth, et al., *Jet Substructure at the Tevatron and LHC: New results, new tools, new benchmarks*, *J.Phys.* **G39** (2012) 063001, [arXiv:1201.0008].

[3] A. Altheimer, A. Arce, L. Asquith, J. Backus Mayes, E. Bergeaas Kuutmann, et al., *Boosted objects and jet substructure at the LHC*, arXiv:1311.2708.

[4] M. H. Seymour, *Searches for new particles using cone and cluster jet algorithms: A Comparative study*, *Z.Phys.* **C62** (1994) 127–138.

[5] J. Butterworth, B. Cox, and J. R. Forshaw, *WW scattering at the CERN LHC*, *Phys.Rev.* **D65** (2002) 096014, [hep-ph/0201098].

[6] J. M. Butterworth, A. R. Davison, M. Rubin, and G. P. Salam, *Jet substructure as a new Higgs search channel at the LHC*, *Phys.Rev.Lett.* **100** (2008) 242001, [arXiv:0802.2470].

[7] L. G. Almeida, S. J. Lee, G. Perez, G. F. Sterman, I. Sung, et al., *Substructure of high-p_T Jets at the LHC*, *Phys.Rev.* **D79** (2009) 074017, [arXiv:0807.0234].

[8] L. G. Almeida, S. J. Lee, G. Perez, I. Sung, and J. Virzi, *Top Jets at the LHC*, *Phys.Rev.* **D79** (2009) 074012, [arXiv:0810.0934].

[9] D. E. Kaplan, K. Rehermann, M. D. Schwartz, and B. Tweedie, *Top Tagging: A Method for Identifying Boosted Hadronically Decaying Top Quarks*, *Phys.Rev.Lett.* **101** (2008) 142001, [arXiv:0806.0848].

[10] G. Brooijmans, *High pt hadronic top quark identification*, Tech. Rep. ATL-PHYS-CONF-2008-008. ATL-COM-PHYS-2008-001, CERN, Geneva, Jan, 2008.

[11] J. Thaler and L.-T. Wang, *Strategies to Identify Boosted Tops*, *JHEP* **0807** (2008) 092, [arXiv:0806.0023].

[12] **CMS Collaboration** Collaboration, *A Cambridge-Aachen (C-A) based Jet Algorithm for boosted top-jet tagging*, Tech. Rep. CMS-PAS-JME-09-001, 2009.

[13] **CMS Collaboration** Collaboration, *Search for High Mass tt Resonances in the All-Hadronic Mode*, Tech. Rep. CMS-PAS-EXO-09-002, 2009.

[14] S. Rappoccio, *A new top jet tagging algorithm for highly boosted top jets*, Tech. Rep. CMS-CR-2009-255, CERN, Geneva, Aug, 2009.

[15] *Reconstruction of high mass $t\bar{t}$ resonances in the lepton+jets channel*, Tech. Rep. ATL-PHYS-PUB-2009-081. ATL-COM-PHYS-2009-255, CERN, Geneva, May, 2009.

[16] G. D. Kribs, A. Martin, T. S. Roy, and M. Spannowsky, *Discovering the Higgs Boson in New Physics Events using Jet Substructure*, *Phys.Rev.* **D81** (2010) 111501, [arXiv:0912.4731].

[17] G. D. Kribs, A. Martin, T. S. Roy, and M. Spannowsky, *Discovering Higgs Bosons of the MSSM using Jet Substructure*, *Phys.Rev.* **D82** (2010) 095012, [arXiv:1006.1656].

[18] C.-R. Chen, M. M. Nojiri, and W. Sreethawong, *Search for the Elusive Higgs Boson Using Jet Structure at LHC*, *JHEP* **1011** (2010) 012, [arXiv:1006.1151].

[19] C. Hackstein and M. Spannowsky, *Boosting Higgs discovery: The Forgotten channel*, *Phys.Rev.* **D82** (2010) 113012, [arXiv:1008.2202].

[20] A. Falkowski, D. Krohn, L.-T. Wang, J. Shelton, and A. Thalapillil, *Unburied Higgs boson: Jet substructure techniques for searching for Higgs' decay into gluons*, *Phys.Rev.* **D84** (2011) 074022, [arXiv:1006.1650].

[21] A. Katz, M. Son, and B. Tweedie, *Jet Substructure and the Search for Neutral Spin-One Resonances in Electroweak Boson Channels*, *JHEP* **1103** (2011) 011, [arXiv:1010.5253].

[22] Y. Cui, Z. Han, and M. D. Schwartz, *W-jet Tagging: Optimizing the Identification of Boosted Hadronically-Decaying W Bosons*, *Phys.Rev.* **D83** (2011) 074023, [arXiv:1012.2077].

[23] J.-H. Kim, *Rest Frame Subjet Algorithm With SISCone Jet For Fully Hadronic Decaying Higgs Search*, *Phys.Rev.* **D83** (2011) 011502, [arXiv:1011.1493].

[24] J. Thaler and K. Van Tilburg, *Identifying Boosted Objects with N-subjettiness*, *JHEP* **1103** (2011) 015, [arXiv:1011.2268].

[25] J. Gallicchio, J. Huth, M. Kagan, M. D. Schwartz, K. Black, et al., *Multivariate discrimination and the Higgs + W/Z search*, *JHEP* **1104** (2011) 069, [arXiv:1010.3698].

[26] J. Gallicchio and M. D. Schwartz, *Seeing in Color: Jet Superstructure*, *Phys.Rev.Lett.* **105** (2010) 022001, [arXiv:1001.5027].

[27] *Prospects for top anti-top resonance searches using early atlas data.*, Tech. Rep. ATL-PHYS-PUB-2010-008, CERN, Geneva, Jul, 2010.

[28] T. Plehn, G. P. Salam, and M. Spannowsky, *Fat Jets for a Light Higgs*, *Phys.Rev.Lett.* **104** (2010) 111801, [arXiv:0910.5472].

[29] T. Plehn, M. Spannowsky, M. Takeuchi, and D. Zerwas, *Stop Reconstruction with Tagged Tops*, *JHEP* **1010** (2010) 078, [arXiv:1006.2833].

[30] L. G. Almeida, S. J. Lee, G. Perez, G. Sterman, and I. Sung, *Template Overlap Method for Massive Jets*, *Phys.Rev.* **D82** (2010) 054034, [arXiv:1006.2035].

[31] J. Thaler and K. Van Tilburg, *Maximizing Boosted Top Identification by Minimizing N-subjettiness*, *JHEP* **1202** (2012) 093, [arXiv:1108.2701].

[32] M. Jankowiak and A. J. Larkoski, *Jet Substructure Without Trees*, *JHEP* **1106** (2011) 057, [arXiv:1104.1646].

[33] A. Hook, M. Jankowiak, and J. G. Wacker, *Jet Dipolarity: Top Tagging with Color Flow*, *JHEP* **1204** (2012) 007, [arXiv:1102.1012].

[34] D. E. Soper and M. Spannowsky, *Finding physics signals with shower deconstruction*, *Phys.Rev.* **D84** (2011) 074002, [arXiv:1102.3480].

[35] L. G. Almeida, O. Erdogan, J. Juknevich, S. J. Lee, G. Perez, et al., *Three-particle templates for a boosted Higgs boson*, *Phys.Rev.* **D85** (2012) 114046, [arXiv:1112.1957].

[36] S. D. Ellis, A. Hornig, T. S. Roy, D. Krohn, and M. D. Schwartz, *Qjets: A Non-Deterministic Approach to Tree-Based Jet Substructure*, *Phys.Rev.Lett.* **108** (2012) 182003, [arXiv:1201.1914].

[37] D. E. Soper and M. Spannowsky, *Finding top quarks with shower deconstruction*, *Phys.Rev.* **D87** (2013), no. 5 054012, [arXiv:1211.3140].

[38] M. Backovic, J. Juknevich, and G. Perez, *Boosting the Standard Model Higgs Signal with the Template Overlap Method*, *JHEP* **1307** (2013) 114, [arXiv:1212.2977].

[39] T. Cohen, E. Izaguirre, M. Lisanti, and H. K. Lou, *Jet Substructure by Accident*, *JHEP* **1303** (2013) 161, [arXiv:1212.1456].

[40] D. Curtin, R. Essig, and B. Shuve, *Boosted Multijet Resonances and New Color-Flow Variables*, *Phys.Rev.* **D88** (2013) 034019, [arXiv:1210.5523].

[41] S. El Hedri, A. Hook, M. Jankowiak, and J. G. Wacker, *Learning How to Count: A High Multiplicity Search for the LHC*, *JHEP* **1308** (2013) 136, [arXiv:1302.1870].

[42] M. Backovic, O. Gabizon, J. Juknevich, G. Perez, and Y. Soreq, *Measuring Boosted Tops in Semi-leptonic $t\bar{t}$ Events for the Standard Model and Beyond*, arXiv:1311.2962.

[43] M. Gouzevitch, A. Oliveira, J. Rojo, R. Rosenfeld, G. P. Salam, et al., *Scale-invariant resonance tagging in multijet events and new physics in Higgs pair production*, *JHEP* **1307** (2013) 148, [arXiv:1303.6636].

[44] A. J. Larkoski, G. P. Salam, and J. Thaler, *Energy Correlation Functions for Jet Substructure*, *JHEP* **1306** (2013) 108, [arXiv:1305.0007].

[45] Y.-T. Chien, *Telescoping Jets: Multiple Event Interpretations with Multiple R's*, arXiv:1304.5240.

[46] D. Kahawala, D. Krohn, and M. D. Schwartz, *Jet Sampling: Improving Event Reconstruction through Multiple Interpretations*, *JHEP* **1306** (2013) 006, [arXiv:1304.2394].

[47] J. Gallicchio and M. D. Schwartz, *Quark and Gluon Tagging at the LHC*, *Phys.Rev.Lett.* **107** (2011) 172001, [arXiv:1106.3076].

[48] J. Gallicchio and M. D. Schwartz, *Quark and Gluon Jet Substructure*, arXiv:1211.7038.

[49] D. Krohn, T. Lin, M. D. Schwartz, and W. J. Waalewijn, *Jet Charge at the LHC*, arXiv:1209.2421.

[50] **CMS Collaboration** Collaboration, S. Chatrchyan et al., *Search for a Higgs boson in the decay channel H to ZZ(*) to q qbar ℓ^- l+ in pp collisions at $\sqrt{s} = 7$ TeV*, JHEP **1204** (2012) 036, [arXiv:1202.1416].

[51] F. Pandolfi and D. Del Re, *Search for the Standard Model Higgs Boson in the $H \to ZZ \to llqq$ Decay Channel at CMS.* PhD thesis, Zurich, ETH, 2012.

[52] M. Cacciari and G. P. Salam, *Pileup subtraction using jet areas*, Phys.Lett. **B659** (2008) 119–126, [arXiv:0707.1378].

[53] D. Krohn, J. Thaler, and L.-T. Wang, *Jet Trimming*, JHEP **1002** (2010) 084, [arXiv:0912.1342].

[54] S. D. Ellis, C. K. Vermilion, and J. R. Walsh, *Techniques for improved heavy particle searches with jet substructure*, Phys.Rev. **D80** (2009) 051501, [arXiv:0903.5081].

[55] S. D. Ellis, C. K. Vermilion, and J. R. Walsh, *Recombination Algorithms and Jet Substructure: Pruning as a Tool for Heavy Particle Searches*, Phys.Rev. **D81** (2010) 094023, [arXiv:0912.0033].

[56] R. Alon, E. Duchovni, G. Perez, A. P. Pranko, and P. K. Sinervo, *A Data-driven method of pile-up correction for the substructure of massive jets*, Phys.Rev. **D84** (2011) 114025, [arXiv:1101.3002].

[57] G. Soyez, G. P. Salam, J. Kim, S. Dutta, and M. Cacciari, *Pileup subtraction for jet shapes*, arXiv:1211.2811.

[58] J. Tseng and H. Evans, *Sequential recombination algorithm for jet clustering and background subtraction*, Phys.Rev. **D88** (2013) 014044, [arXiv:1304.1025].

[59] M. Dasgupta, A. Fregoso, S. Marzani, and G. P. Salam, *Towards an understanding of jet substructure*, JHEP **1309** (2013) 029, [arXiv:1307.0007].

[60] M. Dasgupta, A. Fregoso, S. Marzani, and A. Powling, *Jet substructure with analytical methods*, Eur. Phys. J. C, *73* **11** (2013) 2623, [arXiv:1307.0013].

[61] D. Krohn, M. Low, M. D. Schwartz, and L.-T. Wang, *Jet Cleansing: Pileup Removal at High Luminosity*, arXiv:1309.4777.

[62] **ATLAS Collaboration** Collaboration, D. W. Miller, *Jet substructure in ATLAS*, Tech. Rep. ATL-PHYS-PROC-2011-142, 2011.

[63] **ATLAS Collaboration** Collaboration, G. Aad et al., *Search for resonances decaying into top-quark pairs using fully hadronic decays in pp collisions with ATLAS at $\sqrt{s} = 7$ TeV*, JHEP **1301** (2013) 116, [arXiv:1211.2202].

[64] **ATLAS Collaboration** Collaboration, G. Aad et al., *Search for pair production of massive particles decaying into three quarks with the ATLAS detector in $\sqrt{s} = 7$ TeV pp collisions at the LHC*, JHEP **1212** (2012) 086, [arXiv:1210.4813].

[65] **ATLAS Collaboration** Collaboration, G. Aad et al., *ATLAS measurements of the properties of jets for boosted particle searches*, Phys.Rev. **D86** (2012) 072006, [arXiv:1206.5369].

[66] **ATLAS Collaboration** Collaboration, *Measurement of jet mass and substructure for inclusive jets in s = 7 tev pp collisions with the atlas experiment*, Tech. Rep. ATLAS-CONF-2011-073, CERN, Geneva, May, 2011.

[67] **ATLAS Collaboration** Collaboration, *Light-quark and gluon jets in atlas*, Tech. Rep. ATLAS-CONF-2011-053, CERN, Geneva, Apr, 2011.

[68] **ATLAS Collaboration** Collaboration, G. Aad et al., *Jet mass and substructure of inclusive jets in $\sqrt{s} = 7$ TeV pp collisions with the ATLAS experiment*, JHEP **1205** (2012) 128, [arXiv:1203.4606].

[69] **ATLAS Collaboration** Collaboration, *Studies of the impact and mitigation of pile-up on large-R and groomed jets in ATLAS at $\sqrt{s} = 7$ TeV*, .

[70] **ATLAS Collaboration** Collaboration, *Performance of large-r jets and jet substructure reconstruction with the atlas detector*, Tech. Rep. ATLAS-CONF-2012-065, CERN, Geneva, Jul, 2012.

[71] **ATLAS Collaboration** Collaboration, *Studies of the impact and mitigation of pile-up on large-r and groomed jets in atlas at $\sqrt{s} = 7$ tev*, Tech. Rep. ATLAS-CONF-2012-066, CERN, Geneva, Jul, 2012.

[72] **ATLAS Collaboration** Collaboration, G. Aad et al., *Measurement of jet shapes in top pair events at sqrt(s) = 7 TeV using the ATLAS detector*, arXiv:1307.5749.

[73] **ATLAS Collaboration** Collaboration, G. Aad et al., *Performance of jet substructure techniques for large-R jets in proton-proton collisions at $\sqrt{s} = 7$ TeV using the ATLAS detector*, JHEP **1309** (2013) 076, [arXiv:1306.4945].

[74] **ATLAS Collaboration** Collaboration, *Pile-up subtraction and suppression for jets in ATLAS*, Tech. Rep. ATLAS-CONF-2013-083, ATLAS-COM-CONF-2013-097, 2013.

[75] **ATLAS Collaboration** Collaboration, *Performance of boosted top quark identification in 2012 ATLAS data*, Tech. Rep. ATLAS-CONF-2013-084, ATLAS-COM-CONF-2013-074, 2013.

[76] **ATLAS Collaboration** Collaboration, *Performance of pile-up subtraction for jet shapes*, Tech. Rep. ATLAS-CONF-2013-085, ATLAS-COM-CONF-2013-100, 2013.

[77] **ATLAS Collaboration** Collaboration, *Jet Charge Studies with the ATLAS Detector Using $\sqrt{s} = 8$ TeV Proton-Proton Collision Data*, Tech. Rep. ATLAS-CONF-2013-086, ATLAS-COM-CONF-2013-101, 2013.

[78] **ATLAS Collaboration** Collaboration, *Performance and Validation of Q-Jets at the ATLAS Detector in pp Collisions at $\sqrt{s}=8$ TeV in 2012*, Tech. Rep. ATLAS-CONF-2013-087, ATLAS-COM-CONF-2013-099, 2013.

[79] **ATLAS Collaboration** Collaboration, *Identification and Tagging of Double b-hadron jets with the ATLAS Detector*, .

[80] **CMS Collaboration** Collaboration, *Jet substructure algorithms*, Tech. Rep. CMS-PAS-JME-10-013, CERN, Geneva, 2011.

[81] **CMS Collaboration** Collaboration, *Search for BSM ttbar Production in the Boosted All-Hadronic Final State*, Tech. Rep. CMS-PAS-EXO-11-006, 2011.

[82] **CMS Collaboration** Collaboration, *Measurement of the subjet multiplicity in dijet events from proton-proton collisions at sqrt(s) = 7 tev*, Tech. Rep. CMS-PAS-QCD-10-041, CERN, Geneva, 2010.

[83] **CMS Collaboration** Collaboration, S. Chatrchyan et al., *Measurement of the underlying event activity in pp collisions at $\sqrt{s} = 0.9$ and 7 TeV with the novel jet-area/median approach*, *JHEP* **1208** (2012) 130, [arXiv:1207.2392].

[84] **CMS Collaboration** Collaboration, C. Collaboration, *Performance of quark/gluon discrimination in 8 TeV pp data*, Tech. Rep. CMS-PAS-JME-13-002, 2013.

[85] **CMS Collaboration** Collaboration, C. Collaboration, *Pileup Jet Identification*, Tech. Rep. CMS-PAS-JME-13-005, 2013.

[86] **CMS Collaboration** Collaboration, C. Collaboration, *Performance of b tagging at sqrt(s)=8 TeV in multijet, ttbar and boosted topology events*, Tech. Rep. CMS-PAS-BTV-13-001, 2013.

[87] **CMS Collaboration** Collaboration, C. Collaboration, *Identifying Hadronically Decaying Vector Bosons Merged into a Single Jet*, Tech. Rep. CMS-PAS-JME-13-006, 2013.

[88] **CMS Collaboration** Collaboration, S. Chatrchyan et al., *Shape, transverse size, and charged hadron multiplicity of jets in pp collisions at 7 TeV*, *JHEP* **1206** (2012) 160, [arXiv:1204.3170].

[89] **CMS Collaboration** Collaboration, S. Chatrchyan et al., *Studies of jet mass in dijet and W/Z + jet events*, *JHEP* **1305** (2013) 090, [arXiv:1303.4811].

[90] H.-n. Li, Z. Li, and C.-P. Yuan, *QCD resummation for light-particle jets*, *Phys.Rev.* **D87** (2013) 074025, [arXiv:1206.1344].

[91] S. D. Ellis, C. K. Vermilion, J. R. Walsh, A. Hornig, and C. Lee, *Jet Shapes and Jet Algorithms in SCET*, *JHEP* **1011** (2010) 101, [arXiv:1001.0014].

[92] A. Banfi, M. Dasgupta, K. Khelifa-Kerfa, and S. Marzani, *Non-global logarithms and jet algorithms in high-pT jet shapes*, *JHEP* **1008** (2010) 064, [arXiv:1004.3483].

[93] M. Dasgupta, K. Khelifa-Kerfa, S. Marzani, and M. Spannowsky, *On jet mass distributions in Z+jet and dijet processes at the LHC*, *JHEP* **1210** (2012) 126, [arXiv:1207.1640].

[94] Y.-T. Chien, R. Kelley, M. D. Schwartz, and H. X. Zhu, *Resummation of Jet Mass at Hadron Colliders*, *Phys.Rev.* **D87** (2013) 014010, [arXiv:1208.0010].

[95] T. T. Jouttenus, I. W. Stewart, F. J. Tackmann, and W. J. Waalewijn, *Jet Mass Spectra in Higgs + One Jet at NNLL*, *Phys.Rev.* **D88** (2013) 054031, [arXiv:1302.0846].

[96] M. Rubin, *Non-Global Logarithms in Filtered Jet Algorithms*, *JHEP* **1005** (2010) 005, [arXiv:1002.4557].

[97] J. R. Walsh and S. Zuberi, *Factorization Constraints on Jet Substructure*, arXiv:1110.5333.

[98] I. Feige, M. D. Schwartz, I. W. Stewart, and J. Thaler, *Precision Jet Substructure from Boosted Event Shapes*, *Phys.Rev.Lett.* **109** (2012) 092001, [arXiv:1204.3898].

[99] M. Field, G. Gur-Ari, D. A. Kosower, L. Mannelli, and G. Perez, *Three-Prong Distribution of Massive Narrow QCD Jets*, *Phys.Rev.* **D87** (2013) 094013, [arXiv:1212.2106].

[100] A. J. Larkoski, *QCD Analysis of the Scale-Invariance of Jets*, *Phys.Rev.* **D86** (2012) 054004, [arXiv:1207.1437].

[101] E. Gerwick, S. Schumann, B. Gripaios, and B. Webber, *QCD Jet Rates with the Inclusive Generalized kt Algorithms*, *JHEP* **1304** (2013) 089, [arXiv:1212.5235].

[102] A. J. Larkoski, D. Neill, and J. Thaler, *Jet Shapes with the Broadening Axis*, arXiv:1401.2158.

[103] A. J. Larkoski, I. Moult, and D. Neill, *Toward Multi-Differential Cross Sections: Measuring Two Angularities on a Single Jet*, arXiv:1401.4458.

[104] M. Dasgupta and G. Salam, *Resummation of nonglobal QCD observables*, *Phys.Lett.* **B512** (2001) 323–330, [hep-ph/0104277].

[105] A. J. Larkoski and J. Thaler, *Unsafe but Calculable: Ratios of Angularities in Perturbative QCD*, *JHEP* **1309** (2013) 137, [arXiv:1307.1699].

[106] A. Banfi, G. P. Salam, and G. Zanderighi, *Principles of general final-state resummation and automated implementation*, *JHEP* **0503** (2005) 073, [hep-ph/0407286].

[107] C. F. Berger, T. Kucs, and G. F. Sterman, *Event shape / energy flow correlations*, *Phys.Rev.* **D68** (2003) 014012, [hep-ph/0303051].

[108] M. Cacciari, G. P. Salam, and G. Soyez, *The Catchment Area of Jets*, *JHEP* **0804** (2008) 005, [arXiv:0802.1188].

[109] M. Cacciari, G. P. Salam, and G. Soyez, *The Anti-k(t) jet clustering algorithm*, *JHEP* **0804** (2008) 063, [arXiv:0802.1189].

[110] Y. L. Dokshitzer, G. Leder, S. Moretti, and B. Webber, *Better jet clustering algorithms*, *JHEP* **9708** (1997) 001, [hep-ph/9707323].

[111] M. Wobisch and T. Wengler, *Hadronization corrections to jet cross-sections in deep inelastic scattering*, hep-ph/9907280.

[112] S. Catani, Y. L. Dokshitzer, M. Seymour, and B. Webber, *Longitudinally invariant K_t clustering algorithms for hadron hadron collisions*, *Nucl.Phys.* **B406** (1993) 187–224.

[113] S. D. Ellis and D. E. Soper, *Successive combination jet algorithm for hadron collisions*, *Phys.Rev.* **D48** (1993) 3160–3166, [hep-ph/9305266].

[114] S. Catani, L. Trentadue, G. Turnock, and B. Webber, *Resummation of large logarithms in e+ e- event shape distributions*, *Nucl.Phys.* **B407** (1993) 3–42.

[115] Y. L. Dokshitzer, A. Lucenti, G. Marchesini, and G. Salam, *On the QCD analysis of jet broadening*, *JHEP* **9801** (1998) 011, [hep-ph/9801324].

[116] A. Banfi, G. P. Salam, and G. Zanderighi, *Principles of general final-state resummation and automated implementation*, *JHEP* **0503** (2005) 073, [hep-ph/0407286].

[117] Y. Hatta and T. Ueda, *Resummation of non-global logarithms at finite N_c*, *Nucl.Phys.* **B874** (2013) 808–820, [arXiv:1304.6930].

[118] A. Banfi and M. Dasgupta, *Problems in resumming interjet energy flows with k_t clustering*, *Phys.Lett.* **B628** (2005) 49–56, [hep-ph/0508159].

[119] Y. L. Dokshitzer, G. Marchesini, and G. Oriani, *Measuring color flows in hard processes: Beyond leading order*, *Nucl.Phys.* **B387** (1992) 675–714.

[120] T. Sjostrand, S. Mrenna, and P. Z. Skands, *A Brief Introduction to PYTHIA 8.1*, *Comput.Phys.Commun.* **178** (2008) 852–867, [arXiv:0710.3820].

[121] R. Corke and T. Sjostrand, *Interleaved Parton Showers and Tuning Prospects*, *JHEP* **1103** (2011) 032, [arXiv:1011.1759].

[122] M. Dasgupta, L. Magnea, and G. P. Salam, *Non-perturbative QCD effects in jets at hadron colliders*, *JHEP* **0802** (2008) 055, [arXiv:0712.3014].

[123] M. Cacciari, G. P. Salam, and G. Soyez, *FastJet User Manual*, *Eur.Phys.J.* **C72** (2012) 1896, [arXiv:1111.6097].

[124] M. Cacciari, G. P. Salam, and G. Soyez, *The Catchment Area of Jets*, *JHEP* **0804** (2008) 005, [arXiv:0802.1188].

[125] S. Sapeta, Q. C. Zhang, and Q. C. Zhang, *The mass area of jets*, *JHEP* **1106** (2011) 038, [arXiv:1009.1143].

[126] S. Catani, B. Webber, and G. Marchesini, *QCD coherent branching and semiinclusive processes at large x*, *Nucl.Phys.* **B349** (1991) 635–654.

[127] D. Bertolini, T. Chan, and J. Thaler, *Jet Observables Without Jet Algorithms*, arXiv:1310.7584.

[128] R. Abbate, M. Fickinger, A. H. Hoang, V. Mateu, and I. W. Stewart, *Thrust at N3LL with Power Corrections and a Precision Global Fit for alphas(mZ)*, *Phys.Rev.* **D83** (2011) 074021, [arXiv:1006.3080].